

RESEARCH

Open Access



Preparation and effects of functionalized liposomes targeting breast cancer tumors using chemotherapy, phototherapy, and immunotherapy

Bowen Zeng^{1,2}, Lina Pian^{1,2,3}, Yanhong Liu^{1,2}, Shuangqing Wang^{1,2,4}, Nuoya Wang^{1,2,4}, Chao Liu^{1,2}, Hao Wu^{1,2}, Hongshuang Wan^{1,2}, Liqing Chen^{1,2}, Wei Huang^{1,2}, Zhonggao Gao^{1,2*}, Xuezhe Yin^{3*} and Mingji Jin^{1,2*}

Abstract

Breast cancer therapy has significantly advanced by targeting the programmed cell death-ligand 1/programmed cell death-1 (PD-L1/PD-1) pathway. BMS-202 (a smallmolecule PD-L1 inhibitor) induces PD-L1 dimerization to block PD-1/PD-L1 interactions, allowing the T-cell-mediated immune response to kill tumor cells. However, immunotherapy alone has limited effects. Clinically approved photodynamic therapy (PDT) activates immunity and selectively targets malignant cells. However, PDT aggravates hypoxia, which may compromise its therapeutic efficacy and promote tumor metastasis. We designed a tumor-specific delivery nanoplatform of liposomes that encapsulate the hypoxia-sensitive antitumor drug tirapazamine (TPZ) and the small-molecule immunosuppressant BMS. New indocyanine green (IR820)-loaded polyethylenimine-folic acid (PEI-FA) was complexed with TPZ and BMS-loaded liposomes via electrostatic interactions to form lipid nanocomposites. This nanoplatform can be triggered by near-infrared irradiation to induce PDT, resulting in a hypoxic tumor environment and activation of the prodrug TPZ to achieve efficient chemotherapy. The in vitro and in vivo studies demonstrated excellent combined PDT, chemotherapy, and immunotherapy effects on the regression of distant tumors and lung metastases, providing a reference method for the preparation of targeted agents for treating breast cancer.

Introduction

Breast cancer is the most common malignant tumor and the leading cause of cancer among women worldwide [1, 2]. Current treatment modalities include surgery, radiotherapy, chemotherapy, immunotherapy, and targeted therapy [3]. Immunotherapy is a potent clinical strategy for cancer treatment [4]. The immune checkpoint molecules programmed cell death-1 (PD-1) and programmed cell death-ligand 1 (PD-L1) suppress T-cell activity, enabling tumor cells to elude immune surveillance [5]. PD-1 and PD-L1 inhibitors prevent this immune evasion mechanism, bolstering the immune system's capacity to combat breast cancer cells. Several clinical trials

*Correspondence:

Zhonggao Gao
zggao@imm.ac.cn
Xuezhe Yin
yinxz123@126.com
Mingji Jin
jinmingji@imm.ac.cn

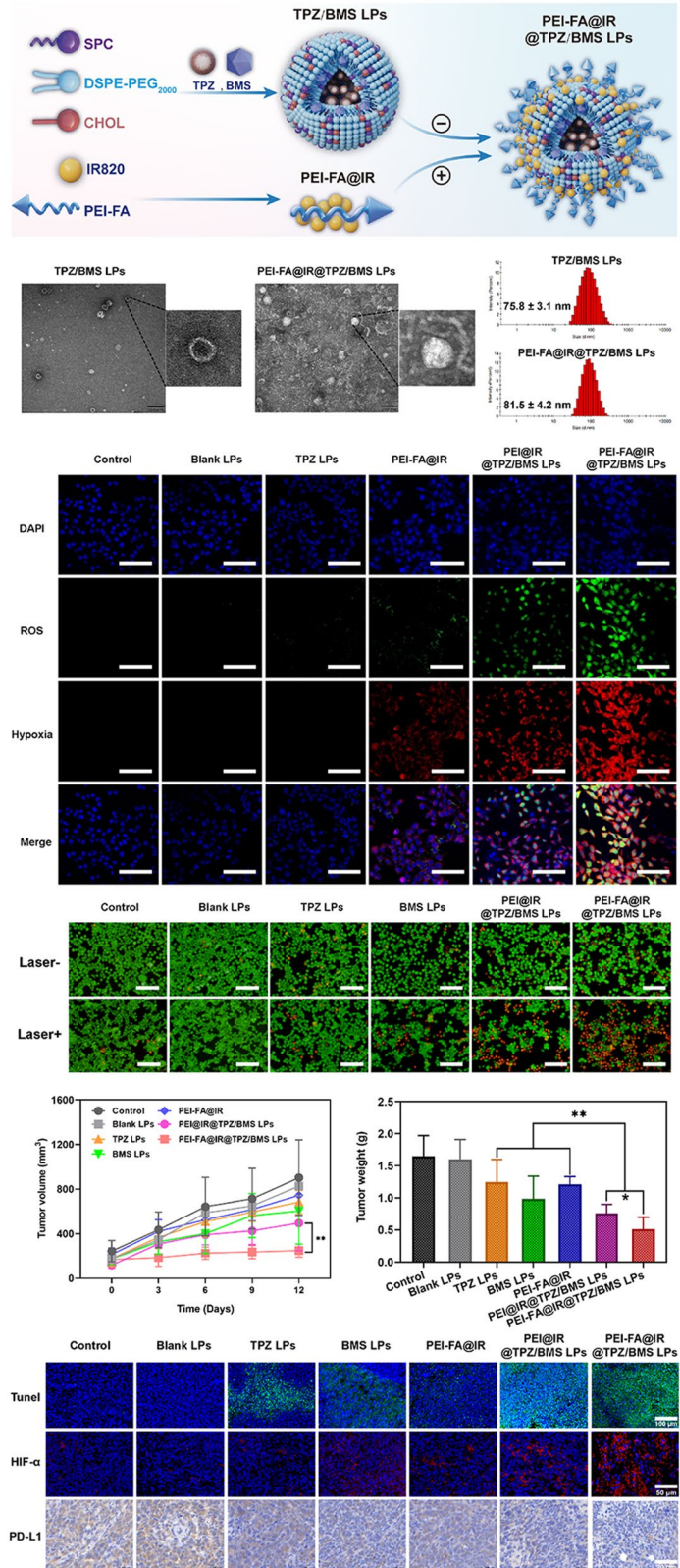
Full list of author information is available at the end of the article



© The Author(s) 2024. **Open Access** This article is licensed under a Creative Commons Attribution-NonCommercial-NoDerivatives 4.0 International License, which permits any non-commercial use, sharing, distribution and reproduction in any medium or format, as long as you give appropriate credit to the original author(s) and the source, provide a link to the Creative Commons licence, and indicate if you modified the licensed material. You do not have permission under this licence to share adapted material derived from this article or parts of it. The images or other third party material in this article are included in the article's Creative Commons licence, unless indicated otherwise in a credit line to the material. If material is not included in the article's Creative Commons licence and your intended use is not permitted by statutory regulation or exceeds the permitted use, you will need to obtain permission directly from the copyright holder. To view a copy of this licence, visit <http://creativecommons.org/licenses/by-nc-nd/4.0/>.

Graphical abstract

Graphical Abstract



Keywords Breast cancer, Photodynamic therapy, Immunotherapy, Immune checkpoint blockade, Folate receptor tumor targeting

confirmed the efficacy of PD-1/PD-L1 inhibitors in the management of advanced breast cancer [6–8]. Combining anti-PD-1/PD-L1 agents with various checkpoint inhibitors, radiotherapy, chemotherapy-targeted therapies, or novel immunotherapies is a crucial avenue of research [9]. Significant strides have been made in cancer treatments with the advent of small-molecule immune suppressors, including BMS-202 (BMS) [10, 11]. BMS is a small molecule inhibitor with strong lipophilic property, which causes dimerization of PD-L1 protein after acting on the surface of PD-L1, thus blocking the binding between PD-1 to PD-L1 and playing immunotherapy.

Photodynamic therapy (PDT) involves the release of reactive oxygen species (ROS) through near-infrared laser irradiation in the presence of photosensitizers [12]. PDT eradicates tumor cells but exhibits minimal toxic effects on adjacent tissues. New indocyanine green (IR820) is a photosensitizer widely used for PDT [13]. PDT induces an immune response through immunogenic cell death (ICD), primarily by inhibiting the PD-L1/PD-1 pathway [14, 15]. PDT induces necrosis or apoptosis in tumor cells, triggering the release of adenosine triphosphate (ATP), high mobility group box 1 (HMGB1), and calreticulin (CRT), which initiate the immune cascade. Combining PDT and small-molecule inhibitors that modulate the checkpoint pathway is an effective photo-immunotherapy against tumors. However, hypoxia induced by oxygen consumption during PDT results in suboptimal responses to PDT and conventional chemoradiotherapy [14]. Tirapazamine (TPZ) is a possible solution to this problem. TPZ is a novel hypoxia-activated bioreductive agent, which is reduced to a cytotoxic metabolite in oxygen-deprived tumor cells. Thus, TPZ selectively damages hypoxic tumor cells while sparing normal cells [15]. TPZ may generate highly toxic reactive metabolites in a hypoxic environment via catalytic electron transfer. The toxic metabolites bind to intracellular DNA, causing damage to purine and pyrimidine residues in double-stranded DNA [16].

Liposomes (LPs) are clinically approved nanoparticles used to deliver various drugs in a sustained and targeted manner [17]. LPs can encapsulate both hydrophilic and hydrophobic drugs and are widely applicable to synergistic therapies. We designed an LPs concurrently encapsulating the hydrophilic hypoxia-activated prodrug TPZ and the hydrophobic small-molecule immunosuppressant BMS. Due to its excellent lipophilicity, BMS can be stably encapsulated in the lipid bilayer of liposomes and act on the same cells together with TPZ embedded in the water-soluble core of liposomes to trigger complementary effects. A positively charged PEI-FA polymer, which can load the negatively charged IR820, was synthesized. Through electrostatic interactions, IR820-loaded PEI-FA was combined with TPZ and BMS-loaded LPs to create a

functionalized tumor-targeting LPs system with distinct drug-carrying compartments (Fig. 1). We hypothesized that this functionalized LPs will bind to folate receptors on the surface of tumor cells via active targeting with FA. Upon exposure to 808 nm light, the photosensitizer IR820 will become excited, generating ROS. The ROS will exacerbate the tumor's hypoxic environment, leading to the conversion of TPZ into its cytotoxic metabolite in the hypoxic milieu. Finally, BMS will bind to PD-L1 in tumor cells to inhibit the interaction between PD-1 and PD-L1, thereby maximizing the anti-tumor effects. This synergistic approach can achieve chemotherapy, phototherapy, and immunotherapy simultaneously. Additionally, the tumor-targeting drug significantly enhances the efficacy of IR820-triggered PDT, while the resulting hypoxic environment activates the therapeutic effect of TPZ and augments the immunotherapy of breast cancer mediated by PDT. This complex LPs delivery system holds significant promise for the treatment of breast cancer.

Materials and methods

Materials

FA, PEI (MW=1.8 kDa), IR820, 1-(3-dimethylaminopropyl)-3-ethylcarbodiimide hydrochloride (EDC), N-hydroxysuccinimide (NHS), coumarin 6 (Cou-6, 98%), and cholesterol were obtained from J&K Scientific Co., Ltd. (Beijing, China). BMS-202 (BMS) was purchased from Dalian Meilun Biotechnology Co., Ltd. (Dalian, China). TPZ was purchased from Shanghai Macklin Biochemical Co., Ltd. (Shanghai, China). Soybean Phospholipid (SPC) and DSPE-PEG₂₀₀₀ (MW 2794.07 Da) were obtained from AVT Pharmaceutical Technology Co., Ltd. (Shanghai, China). The Cell Counting Kit-8 (CCK-8) was obtained from Dojindo Laboratories (Kumamoto, Japan). Annexin V-FITC/PI apoptosis detection kit was obtained from 4 A Biotech Co., Ltd. (Beijing, China). The ROS-ID[®] Hypoxia/Oxidative Stress Detection Kit was purchased from Enzo Life Sciences Co., Ltd. (Beijing, China). The Calcineurin-AM/PI Staining Kit and DAPI were purchased from Solarbio Life Sciences Co., Ltd. (Beijing, China). DIR was purchased from Biotium Inc. (Hayward, CA, USA). Mouse Tumor Necrosis Factor Alpha (TNF- α) ELISA Kit and Mouse Interferon Gamma (IFN- γ) ELISA Kits were obtained from Wuhan Fine Biotech Co., Ltd. (Wuhan, China). Chloroform and methanol (HPLC grade) were purchased from Sigma-Aldrich Co. (St. Louis, MO, USA). All other chemicals were of analytical purity and used without further purification.

Fetal bovine serum (FBS) was purchased from GIBCO LLC. (Grand Island, NY, USA). RPMI 1640 medium and phosphate-buffered saline (PBS) were obtained from Thermo Fisher Scientific Co., Ltd. (Beijing, China). APC anti-mouse CD45 (103112), Alexa Fluor[®] 700

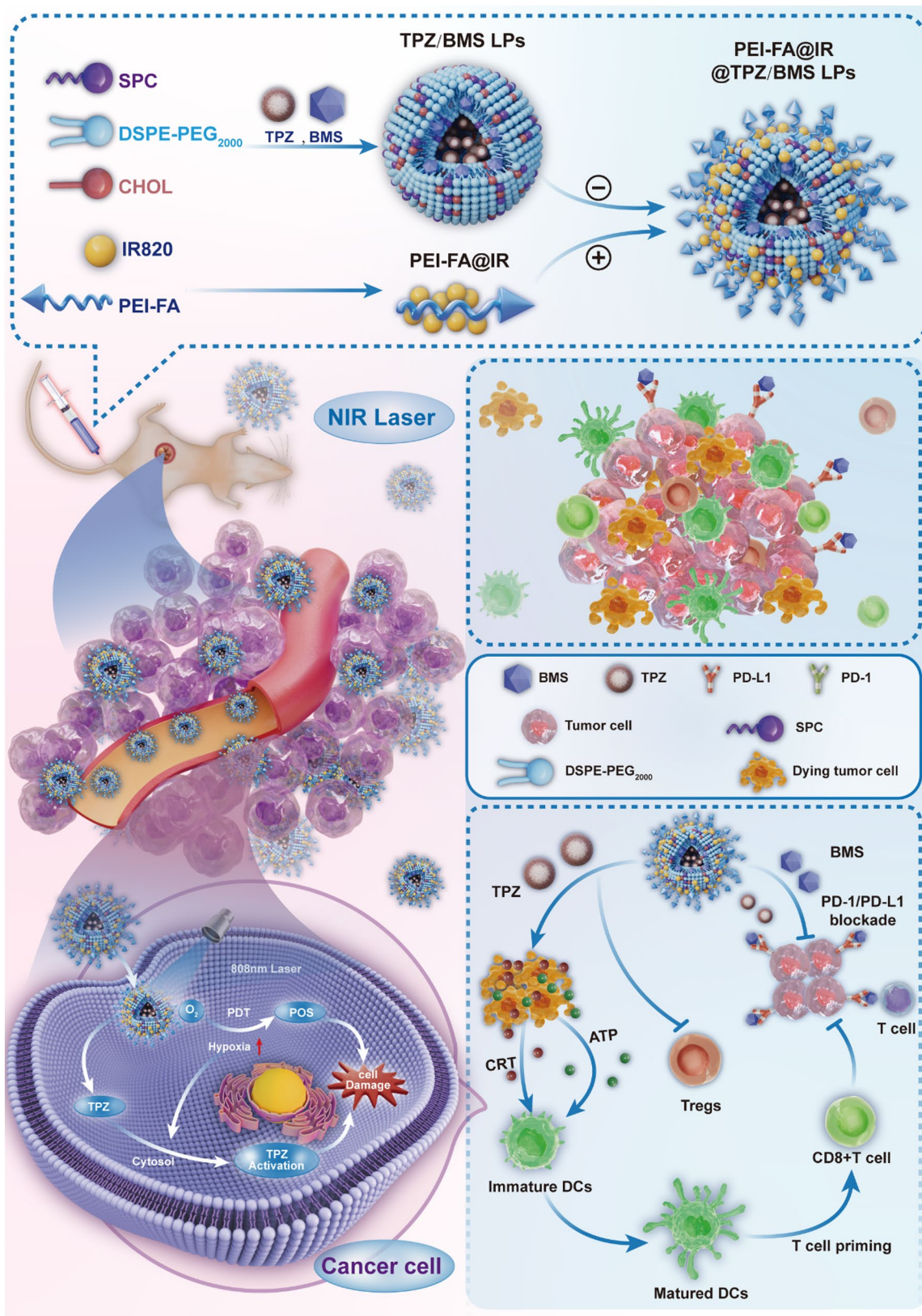


Fig. 1 Schematic illustration of the preparation of PEI-FA@IR@TPZ/BMS LPs and light-triggered hypoxia-activated effects on of chemotherapy, phototherapy and immunotherapy of on tumors

anti-mouse CD3 (100216), PE/Dazzle™ 594 anti-mouse CD4 (100456), FITC anti-mouse CD8a (100706), Pacific Blue™ anti-mouse FOXP3 (126410), Brilliant Violet 421™ anti-mouse CD86 (105032), and RBC Lysis Buffer (10X, 420302) were obtained from BioLegend (San Diego, CA, USA). PE Rat Anti-Mouse CD25 (553866) and PE Hamster Anti-Mouse CD11c (557401) were obtained from BD Biosciences (San Jose, CA, USA). The Foxp3/Transcription Factor Staining Buffer Kit was purchased from Tonbo Biosciences (San Diego, CA, USA).

Cell line and animals

The 4T1, A2780 and bEND.3 cells were obtained from the Department of Pathology at the Institute of Medicinal Biotechnology at Peking Union Medical College (PUMC). The cells were cultured in RPMI 1640 medium supplemented with 10% FBS at 37 °C and 5% CO₂.

BALB/C mice 6–8 weeks, female, 16 ± 2 g) were obtained from Vital River Laboratory Animal Technology Co. Ltd. (Beijing, China). All animal experiments were conducted following the guidelines prepared and approved by the Laboratory Animal Ethics Committee of the Institute of Materia Medica in CAMS and PUMC (Animal Ethics NO. 00003868).

Synthesis and characterization of PEI-FA

The amino group of PEI_{1.8k} was linked to the carboxyl group of FA via an amidation reaction. Briefly, 66 mg of FA (0.15 mmol), 69 mg of NHS (0.6 mmol), and 115 mg of EDC (0.6 mmol) were dissolved in 10 mL of DMSO. The carboxyl group of FA was activated by stirring for 4 h at room temperature with light and nitrogen protection. The product was slowly added dropwise to the PEI_{1.8k} (0.15 mmol) while stirring. The resulting product was extracted and enriched with 10 times the volume of acetone. The precipitate was washed three times with acetone and dialyzed (MWCO: 2500) for 48 h to remove unreacted FA. The final product was obtained by freeze-drying. The structure of PEI-FA was analyzed using ¹H-NMR (400 MHz, Varian Medical Systems, Inc., Palo Alto, CA, USA) and Fourier-transform infrared spectroscopy (FTIR) (Nicolet 5700, Beijing, China).

Preparation of PEI-FA@IR@TPZ/BMS liposomes

SPC, DSPE-PEG₂₀₀₀, Cholesterol, and BMS (at a mass ratio of 8:7:2:1) were dissolved in chloroform and dried using a rotary evaporator. A thin film was formed by adding this mixture to 2 mL of PBS solution containing 2 mg of TPZ and hydrating for 1 h at 45 °C with agitation at 120 rpm. The mixture was sonicated at 65 W for 10 min, with 2 s of sonication followed by 2 s of rest in an ice bath, using an ultrasonic cell pulverizer (Scientz 950E; Ningbo Scientz Biotechnology Co., Ltd., Zhejiang, China). Dual-drug LPs, referred to as TPZ/BMS LPs, were formed.

IR820 and PEI-FA (1:2 mass ratio) were dissolved in deionized water. The PEI-FA@IR mixture was mixed with TPZ/BMS LPs and stirred with light protection for 24 h. After the 0.22 μm filter membrane is passed, the final product is obtained by centrifuge at 25,000 rpm for 30 min with 100,000 molecular weight cut-off. A blank vector (Blank LPs), TPZ-loaded LPs (TPZ LPs), BMS-loaded LPs (BMS LPs), IR820 with PEI-FA (PEI-FA@IR), and TPZ/BMS LPs with IR820 and PEI (PEI@IR@TPZ/BMS LPs) were prepared using the same methods described earlier. All samples were stored at 4 °C.

Characterization

The mean particle size, polydispersity index (PDI), and zeta potential of TPZ/BMS LPs and PEI-FA@IR@TPZ/BMS LPs were measured using dynamic light scattering (DLS) and electrophoretic light scattering (Zetasizer Nano ZS90; Malvern Instruments Ltd., UK). The morphology of TPZ/BMS LPs and PEI-FA@IR@TPZ/BMS LPs were characterized using transmission electron microscopy (TEM, JEM-1400PLUS, JEOL Ltd., Tokyo, Japan) [18]. The unencapsulated BMS was removed by passing PEI-FA@IR@TPZ/BMS LPs through a 0.22 μm Millipore membrane filter during the preparation. The concentrations of BMS and TPZ were determined using high performance liquid chromatography (HPLC, Agilent 1200 infinity; Agilent Technologies, Santa Clara, CA, USA) and UV-Vis spectrophotometry (TU-1810, Pulse Analyzer General Instrument Ltd., Beijing, China), respectively [19]. BMS was detected at 210 nm using a mobile phase of methanol and water (70:30). TPZ was detected at 460 nm. The encapsulation efficiency of PEI-FA@IR@TPZ/BMS LPs was determined using ultracentrifugation at 20,000 rpm for 60 min. The encapsulation efficiency rate (EE%) of PEI-FA@IR@TPZ/BMS LPs was calculated with the following formula:

$$EE\% = \frac{\text{Weight of encapsulated drug}}{\text{Weight of total drug}} \times 100\%$$

To determine the stability of PEI-FA@IR@TPZ/BMS LPs, the prepared solution was stored at 4 °C for 7 days in PBS or PBS containing 50% of serum. The color, transparency, particle size, zeta potential, and PDI of PEI-FA@IR@TPZ/BMS LPs were recorded during the 7 days.

The release of PEI-FA@IR@TPZ/BMS LPs was evaluated in PBS (pH 7.4) using dialysis method. Briefly, 1 mL of free BMS, free TPZ or PEI-FA@IR@TPZ/BMS LPs was added to the dialysis bags (MWCO, 10000 kDa) and then immersed in 10 mL of PBS medium containing 0.5% Tween 80 and shaken at 100 rpm at 37 °C (TPZ: 0.33 μg/mL; BMS: 1 μg/mL). At the indicated times, 1 mL aliquots were extracted and supplemented with the same volume of fresh medium. The concentrations of TPZ and

BMS were determined using UV spectrophotometry and HPLC, as described earlier.

Cellular uptake analysis

The time-dependent cellular uptake of PEI-FA@IR@TPZ/BMS LPs was determined using 4T1 cells. Cells (10×10^4 cells/mL/well at the logarithmic growth stage) were seeded into 12-well plates. After 24 h of incubation, the medium was replaced with fresh culture medium containing PEI-FA@IR@TPZ/BMS LPs (TPZ: 0.33 $\mu\text{g/mL}$; BMS: 1 $\mu\text{g/mL}$). After incubation for 5, 10, and 30 min, the cells were irradiated with an 808 nm laser (0.5 W/cm^2) for 10 min. The cells were washed three times with cold PBS and fixed with 4% paraformaldehyde. The nuclei were labeled with DAPI, and fluorescence was observed using a confocal laser scanning microscope (CLSM, Carl Zeiss LSM 710; Carl Zeiss Microscope, Jena, Germany). The uptake efficiency of PEI-FA@IR@TPZ/BMS LPs by 4T1 cells was quantitatively evaluated by flow cytometry. Briefly, the cells were incubated with PEI-FA@IR@TPZ/BMS LPs for 5, 10, and 30 min, respectively. Subsequently, the cells were rinsed, harvested and analyzed using flow cytometry (Becton Dickinson, Franklin Lake, NJ, USA).

A qualitative evaluation of 4T1 cell uptake was also performed. The green fluorescent probe cou-6-labeled liposomes were constructed to visualize the cellular uptake and localization of nanoparticles in 4T1 cells. The cells were seeded into 12-well plates (10×10^4 cells/mL). After incubating for 24 h, cells were treated with serum-free media containing free Cou-6, Cou-6 LPs, PEI@Cou-6 LPs or PEI-FA@Cou-6 LPs (with a Cou-6 concentration of 1 $\mu\text{g/mL}$). After 2 h of incubation, cells were washed three times with cold PBS, fixed with 4% paraformaldehyde, and the nuclei were labeled with DAPI solution. Cell uptake was observed with CLSM. To further confirm the targeted uptake efficiency of PEI-FA@IR@TPZ/BMS LPs in 4T1 cells, the cells were incubated with free Cou-6, Cou-6 LPs, PEI@Cou-6 LPs or PEI-FA@Cou-6 LPs for 4 h. Then, the cells were collected and analyzed using flow cytometry.

The active targeting efficacy of FA-based imaging towards 4T1, A2780, bEND.3 cells were confirmed with CLSM analysis. 4T1, A2780, bEND.3 cells were seeded onto coverslips in a 12-well plate at a density of 10×10^4 cells per well and incubated at 37°C to allow cell attachment. After 24 h, each group of cells was pretreated with free FA (10 mg/mL) for 1 h to block the FA receptors. Then, PEI-FA@Cou-6 LPs were treated to cells for 2 h. After washed with PBS, cells were fixed with 4% paraformaldehyde for 15 min. Cells were then observed with a confocal microscope (Carl Zeiss LSM 710, Carl Zeiss Microscopy GmbH, Germany).

In vitro ROS and hypoxia detection

While undergoing PDT, cancer cells produce singlet oxygen and other ROS upon activation of IR820 by irradiation, followed by increasing hypoxia in the surrounding area [20]. To evaluate ROS and hypoxia, 4T1 cells were seeded into 12-well plates (10×10^4 cells/well) and cultured for 24 h. The cells were then treated with Blank LPs, TPZ LPs, PEI-FA@IR, PEI@IR@TPZ/BMS LPs, or PEI-FA@IR@TPZ/BMS LPs (0.3 $\mu\text{g/ml}$ and 1 $\mu\text{g/ml}$ for TPZ and BMS, respectively). After irradiating the cells with an 808 nm laser (0.5 W/cm^2) for 10 min, the cells were incubated with the hypoxia detection solution for 30 min in the dark. Finally, the cells were treated according to the instructions in the kit and photographed using CLSM. The CLSM data were analyzed using ImageJ.

CCK-8 assay

The cytotoxicity of blank vectors was evaluated using the CCK-8 assay. The 4T1 cells (4×10^3 cells/well at the logarithmic growth stage) were seeded into 96-well plates and cultured for 24 h. The cells were then treated with different concentrations of Blank LPs or PEI-FA@Blank LPs for 24 and 48 h, followed by treatment with 200 μL of a serum-free medium containing 10% CCK-8 for 3 h at 37°C . The optical density (OD) values were measured at 450 nm using a Synergy H1 Microplate Reader (BioTek Instruments, Inc., Winooski, VT, USA). Cell viability was calculated using the following equation:

$$\text{Cell viability (\%)} = \frac{(A_{\text{treatments}} - A_{\text{blank}})}{(A_{\text{control}} - A_{\text{blank}})} \times 100\%$$

$A_{\text{treatments}}$ and A_{control} represented the absorbance value of the treatment groups and control group, respectively. A_{blank} represented the absorbance value of blank wells. The inhibition of cell proliferation was also assessed. After 24 h of cell culture, the cells were treated with Blank LPs, TPZ LPs, BMS LPs, PEI@IR@TPZ/BMS LPs, or PEI-FA@IR@TPZ/BMS LPs (0.3 $\mu\text{g/ml}$ and 1 $\mu\text{g/ml}$ for TPZ and BMS, respectively) for 2 h. The cells were irradiated with an 808 nm laser (0.5 W/cm^2) for 10 min per well. After 24 h, the inhibition of cell growth was evaluated.

Cell apoptosis assay

Cell apoptosis was evaluated using an Annexin V-FITC/PI kit. The 4T1 cells (10×10^4 cells/mL) were seeded into 12 well plates and cultures for 24 h. The cells were treated with Blank LPs, TPZ LPs, BMS LPs, PEI@IR@TPZ/BMS LPs, or PEI-FA@IR@TPZ/BMS LPs (0.3 $\mu\text{g/ml}$ and 1 $\mu\text{g/ml}$ for TPZ and BMS, respectively) for 4 h after, followed by irradiation with an 808 nm laser (0.5 W/cm^2) for 10 min. After 24 h, the cells were washed with PBS, treated with trypsin (without EDTA), centrifuged

at 500×g for 5 min, and stained with FITC and PI. The stained cells were analyzed using a FACS Calibur flow cytometer (Becton Dickinson, Franklin Lake, NJ, USA).

Calcein-AM/PI double staining assay

The 4T1 cells (4×10^4 cells/well) were seeded into 24-well plates and cultured for 24 h. Cells were treated with Blank LPs, TPZ LPs, BMS LPs, PEI@IR@TPZ/BMS LPs, or PEI-FA@IR@TPZ/BMS LPs (0.3 µg/ml and 1 µg/ml for TPZ and BMS, respectively) in serum-free medium for 4 h followed by irradiation with an 808 nm laser (0.5 W/cm^2) for 10 min. After 24 h, the cells were washed with cold PBS, fixed with 4% paraformaldehyde for 20 min, and treated according to the instructions for the Calcein-AM/PI Live/Dead Cell staining kit. The fluorescence images of live cells and dead cells were captured using an IX51 inverted fluorescence microscope (Olympus Corporation, Tokyo, Japan), and the data were analyzed with ImageJ.

Analysis of in vitro ICD biomarkers

To evaluate the in vitro ICD biomarker levels, 4T1 cells (1×10^5 cells/well) were seeded into 12-well plates. After 24 h, the cells were treated with Blank LPs, TPZ LPs, BMS LPs, PEI@IR@TPZ/BMS LPs, or PEI-FA@IR@TPZ/BMS LPs for 4 h, followed by irradiation with an 808 nm (0.5 W/cm^2) laser for 10 min. After 24 h, the cells were washed with PBS, fixed with 4% paraformaldehyde for 10 min, and washed with PBS. The cells were incubated with anti-CRT (ab92516, 1:800) as the primary antibody for 4 h at 37 °C. The secondary antibodies conjugated with a fluorescence probe were added and incubated for 1 h. The cell nuclei were stained with DAPI for 15 min, and the cells were observed using CLSM.

To evaluate HMGB1 and ATP levels in the media, the 4T1 cells were treated as described earlier. Controls were not exposed to irradiation. Supernatants were collected and centrifuged at 3000 rpm for 10 min to remove cellular debris. The released HMGB1 in cell supernatants was detected using an HMGB1 ELISA kit, and the released ATP in cell supernatants was detected using an ATP Content Assay Kit according to the manufacturer's instructions (HMGB1 and ATP ELISA kits, Beyotime Biotechnology Co., Ltd., Shanghai, China).

In vivo imaging and bio-distribution analysis

The biological distribution and tumor accumulation of the lipid nanoparticles after systemic administration were investigated using an in vivo imaging system. We prepared PEI@IR@TPZ/BMS LPs and PEI-FA@IR@TPZ/BMS as described before. To develop triple-negative breast cancer-bearing orthotopic mouse model, 4T1 cells (2×10^6) in PBS were injected into the right mammary gland of each mouse. Tumor volume (V) was calculated

as follows: $V = (a^2 \times b)/2$ (where a represents the tumor width, and b represents the tumor length). When the tumor volume reached 200 mm^3 , mice were randomly divided into two groups ($n=3/\text{group}$). PEI@IR@TPZ/BMS LPs and PEI-FA@IR@TPZ/BMS LPs were administered through the tail vein at IR dose of 1.5 mg/kg. At 2, 4, 6, 8, 12, and 24 h after injection, mice were anesthetized and imaged using an in vivo imaging system (Caliper Life Sciences Inc., Mountain View, CA, USA). After 24 h, the mice were euthanized. The heart, liver, spleen, lung, kidney, and tumor tissues were dissected and isolated. The regions of interest were analyzed using Living Image software (Version 4.3.1; Caliper Life Sciences Inc.).

In vivo US-induced ROS generation

To evaluate US-induced ROS generation at the tumor sites, the tumor-bearing BALB/c mice ($n=3/\text{group}$) were intravenously injected with PBS or PEI-FA@IR@TPZ/BMS LPs (TPZ, 1 mg/kg; BMS, 3 mg/kg). After 24 h, the mice were anesthetized with chloral hydrate and injected with 50 µg DCFH-DA intra-tumorally. After 10 min, the tumor sites of the mice were irradiated (808 nm, 0.5 W/cm^2) for 10 min and then, the mice were sacrificed. The tumors were collected and flash frozen, counterstained with DAPI, and observed by CLSM.

In vivo anti-tumor evaluation

BALB/c mice with almost 100 mm^3 tumor volumes were randomly divided into the following seven groups ($n=5/\text{group}$): saline, Blank LPs, TPZ LPs, BMS LPs, PEI-FA@IR, PEI@IR@TPZ/BMS LPs, and PEI-FA@IR@TPZ/BMS LPs (TPZ, 1 mg/kg; BMS, 3 mg/kg). The drugs were administered every 3 days. The tumor sites of the mice in the light group were irradiated (808 nm, 0.5 W/cm^2) for 10 min on the second day after administration, for a total of four administrations. On day 15, mice were sacrificed, and tumors and major organs, including the heart, livers, spleen, lung, and kidney, were harvested. The tumors were sectioned and stained with hematoxylin&eosin (H&E) and terminal deoxynucleotidyl transferase dUTP nick-end labeling (TUNEL). Hypoxia-inducible factor-1 α (HIF-1 α) and PD-L1 expression in tumor tissues was detected by immunohistochemistry (IHC), and lung tissues were fixed in Bouin's solution followed by photographic observation of metastases. Blood was centrifuged at 4000 rpm for 10 min, and serum was collected for the measurement of blood urea nitrogen, creatinine, aspartate aminotransferase, and alanine aminotransferase.

In vivo immune response analysis

To study the proliferation and functionality of immune cells in vivo after treatment, tumor tissues and spleens were collected from the different treatment groups (as described earlier). Immune cells were analyzed using

flow cytometry. Helper T cells (Ths, CD3+CD4+CD8-), cytotoxic T lymphocytes (CTLs, CD3+CD4-CD8+), and regulatory T cells (Tregs, CD4+CD25+Foxp3+) were stained, according to the manufacturers' instructions, with the following fluorochrome-containing antibodies: APC-anti-mouse-CD45, Alexa Fluor® 700-anti-mouse-CD3, PE/Dazzle™ 594-anti-mouse-CD4, FITC-anti-mouse-CD8a, PE-Rat Anti-Mouse-CD25, and Pacific Blue™-anti-mouse-FOXP₃. The stained cells were analyzed using flow cytometry (Becton Dickinson, Franklin Lakes, NJ, USA) with FlowJo 10.4 software. Splenic dendritic cells (DCs, CD45+CD11c+CD86+) were fluorescently labeled with APC-anti-mouse-CD45, PE-Hamster Anti-Mouse-CD11c, and Brilliant Violet 421™-anti-mouse-CD86 antibodies.

To detect treatment-induced cytokine secretion, whole mouse blood was collected after treatment. Serum concentrations of TNF- α and IFN- γ were measured using ELISA kits according to the manufacturer's instructions. In addition, IHC analysis was performed for CD8 and CRT expressed by the tumor.

Statistical analyses

All the results were presented as the mean \pm standard deviation (SD). Data were analyzed using Student's t-test or one-way ANOVA followed by Tukey's post-test. Statistical significance was set as * P <0.05, ** P <0.01, and *** P <0.001.

Results and discussion

Synthesis and characterization of PEI-FA

PEI-FA was synthesized through the amidation reaction between the carboxyl group of FA and the amino group of PEI, as illustrated in Figure S1(A). As shown by the ¹H NMR spectra (Figure S1(B)), a proton signal at δ =3.5 ppm on the PEI chain indicated the amide bond [21, 22], and the proton peak of the benzene ring on FA in the range of δ =6.7–9 ppm confirmed the successful coupling of FA to PEI via the amide bond [23]. Moreover, the chemical bond between PEI and FA was confirmed by the strong absorption peak at 1643 cm⁻¹ (strong absorption of formed -NH group) in the FTIR (Figure S1(C)) [24].

Characterization of liposomes

The particle size and PDI of PEI-FA@IR@TPZ/BMS LPs were determined using DLS, as shown in Fig. 2A. The TPZ/BMS LPs exhibited a particle size of 75.8 \pm 3.1 nm (PDI of 0.20 \pm 0.03) and a zeta potential of -25.1 \pm 2.7 mV. After coating with PEI-FA@IR, the particle size of PEI-FA@IR@TPZ/BMS LPs had little change (81.5 \pm 4.2 nm), but the zeta potential became 7.11 \pm 5.0 mV due to the strong positive effect of PEI-FA coating. As shown by TEM, the TPZ/BMS LPs exhibited a small particle size, uniform distribution, and smooth, round surface of

typical liposome structure (Fig. 2D). And an additional layer outside PEI-FA@IR composite liposomes were also confirmed the uniform, round shape consistent with the particle size measurements. And it can be seen that there is a white shell covering the surface of the liposome, which is the PEI-FA@IR outer layer that is coated on the surface of TPZ/BMS LPs.

The EE% of the prepared PEI-FA@IR@TPZ/BMS LPs were 98.1% for BMS and 31.3% for TPZ. The stability of PEI-FA@IR@TPZ/BMS LPs under PBS or PBS containing 50% serum was assessed over 7 days, while the PEI-FA@IR@TPZ/BMS LPs were stored at 4 °C. The solution remained clear with no observable drug precipitation during the 7 days (Figure S2). The particle size and zeta potential of the LPs did not change significantly (Fig. 2B and C). Moreover, the successful encapsulation of TPZ and IR820 was confirmed by the characteristic UV-VIS absorption peaks at 460 nm and 820 nm, respectively (Fig. 2E). The release rate of free TPZ and free BMS is rapid and burst. The release rate of TPZ within 24 h is nearly 100%, and the release rate of BMS within 24 h is also about 70%. However, after liposomal encapsulation, TPZ and BMS were obviously released in a sustained-state, with less than 30% released of BMS and less than 50% release of TPZ within 12 h (Fig. 2F and G).

Cellular uptake

The uptake of PEI-FA@IR@TPZ/BMS LPs by 4T1 cells was assessed using CLSM and flow cytometry. Cells exhibited a time-dependent uptake of PEI-FA@IR@TPZ/BMS LPs after irradiation. As shown in Fig. 3A, the fluorescence intensity of TPZ increased over time, and 4T1 cells treated with laser-activated PEI-FA@IR@TPZ/BMS LPs displayed higher fluorescence signals than other treatment groups. Flow cytometry confirmed these findings, as shown in Fig. 3B and C. The fluorescence intensity at 30 min of incubation was 1.2-fold and 1.14-fold higher than the intensity at 5 and 10 min of incubation. The fluorescent signals were stronger in cells treated with Cou-6 LPs and PEI-FA@Cou-6 LPs than in cells treated with Free Cou-6, consistent with flow cytometry results (Fig. 3D, E, and G). The fluorescence intensity of cells treated with PEI-FA@Cou-6 LPs was 4.84-fold higher than the fluorescence intensity of cells treated with Cou-6 LPs. Notably, PEI-FA@Cou-6 LPs exhibited the highest cellular uptake efficiency in 4T1 cells, demonstrating the active targeting effect facilitated by FA and providing the basis for subsequent experiments.

FA receptor is mainly highly expressed in some substantial tumor tissues, but not expressed or expressed at a very low level in normal tissues. So we selected ovarian cancer cell line A2780 with high expression of FA receptor and mouse brain microvascular endothelial cell line bEND.3 with relatively low expression of FA receptor

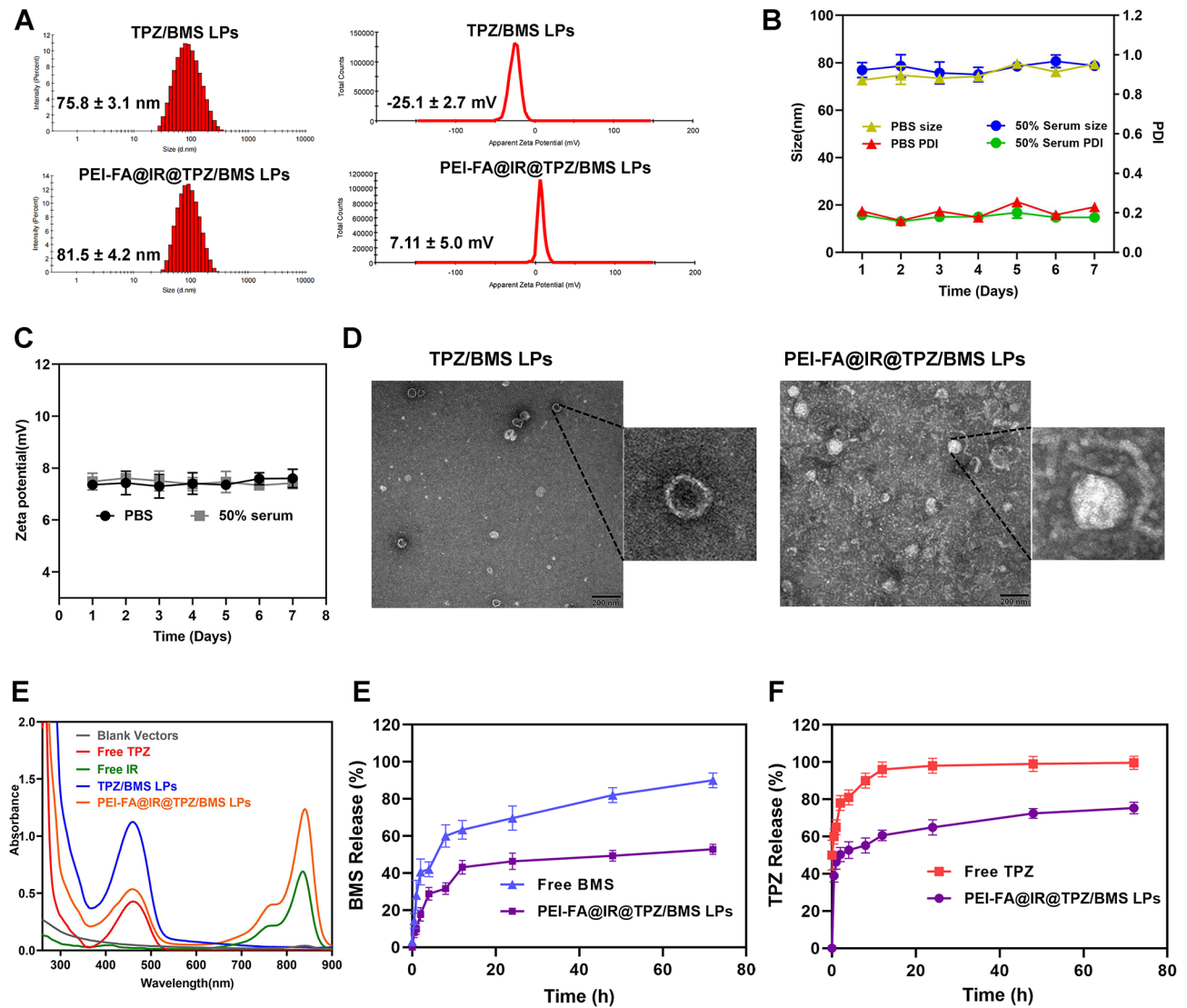


Fig. 2 Characterization of TPZ/BMS LPs and PEI-FA@IR@TPZ/BMS LPs. **(A)** The average size and Zeta potential of TPZ/BMS LPs and PEI-FA@IR@TPZ/BMS LPs. **(B)** Particle size and PDI changes of PEI-FA@IR@TPZ/BMS LPs in PBS or PBS containing 50% of serum within 7 days. **(C)** Zeta potential changes of PEI-FA@IR@TPZ/BMS LPs in PBS or PBS containing 50% of serum within 7 days. **(D)** TEM images of TPZ/BMS LPs and PEI-FA@IR@TPZ/BMS LPs (Scale bar: 200 nm). **(E)** UV/Vis absorption spectra. **(F)** The drug release behavior of BMS within 72 h. **(G)** The drug release behavior of TPZ within 72 h

to investigate the uptake of FA-modified liposomes. As shown in Fig. 3E and H, the results showed that there was no difference in liposome uptake in bEND.3 cells in groups with or without pre-incubated FA. In A2780 cells and 4T1 cell lines, liposome uptake and fluorescence intensity were significantly increased in the group without FA incubation compared with that in the group with FA incubation in advance, indicating that FA modified liposomes could bind specifically to tumor cells with high expression of FA receptor.

In vitro ROS/hypoxia detection

When excited by 808 nm infrared irradiation, IR820 generates ROS, consuming oxygen in tumor tissue and intensifying the existing hypoxic conditions. In this

microenvironment, TPZ becomes activated, resulting in free radical-mediated oxidative DNA damage and tumor cell death. The generation of ROS and the induction of hypoxia were measured in 4T1 cells treated with LPs after laser irradiation. As shown in Fig. 4A, the control group exhibited minimal ROS (green) or hypoxia (red). In contrast, cells treated with PEI-FA@IR@TPZ/BMS LPs displayed a substantial increase in ROS production and hypoxia after 808 nm laser irradiation. As can be seen from the quantitative analysis results of Fig. 4B, the heightened cellular uptake of PEI-FA@IR@TPZ/BMS LPs induced increased ROS production and subsequent hypoxia, suggesting that the LPs enhanced the anticancer activity of TPZ.

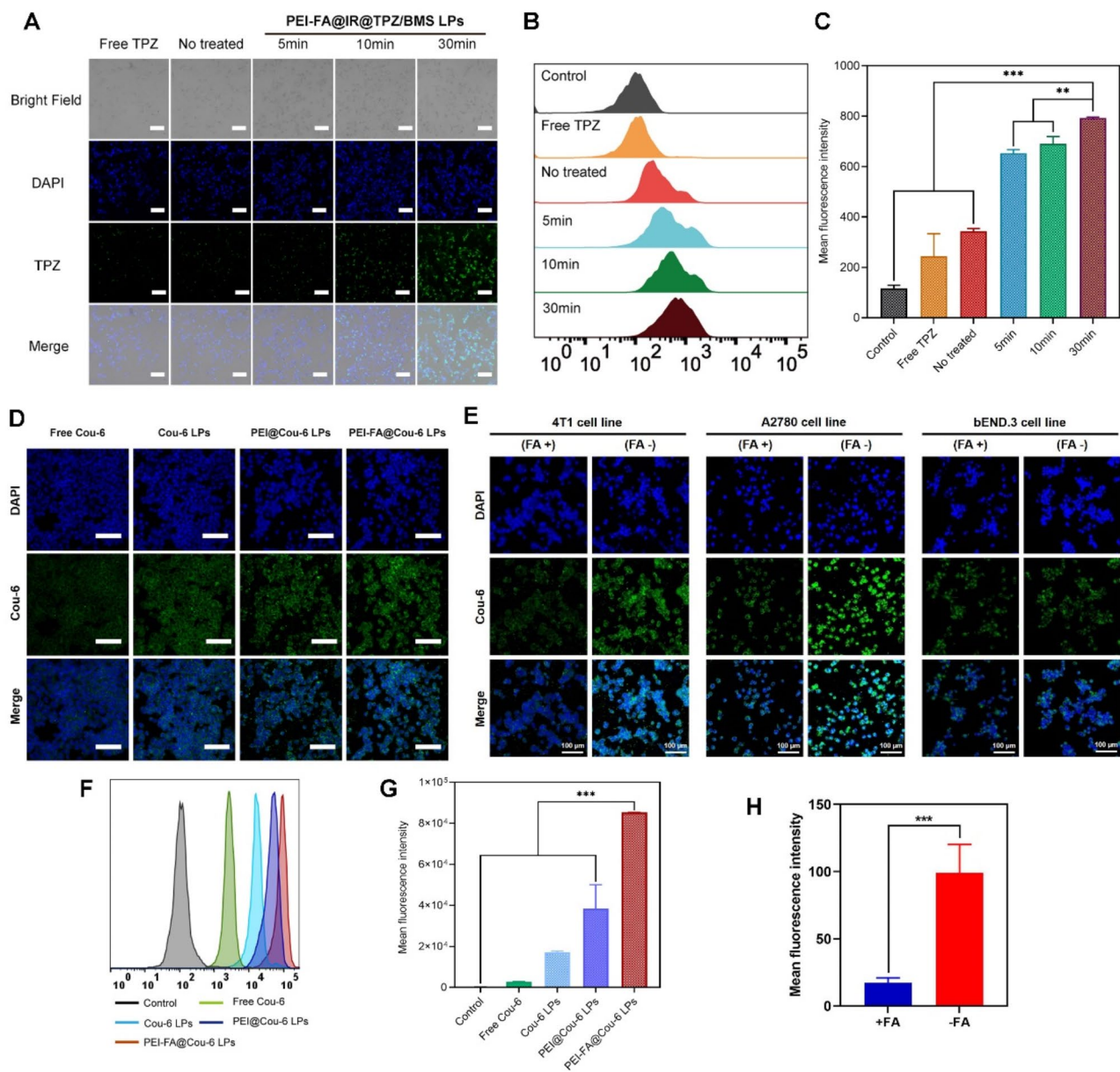


Fig. 3 In vitro cellular uptake (A) Observation of 4T1 cells after treatment with PEI-FA@IR@TPZ/BMS LPs under irradiation within 30 min (Scale bar: 100 μ m). (B) Cellular uptake and (C) the mean fluorescence intensity analysis of PEI-FA@IR@TPZ/BMS LPs incubated with 4T1 cells by flow cytometry within 30 min. (D) Cellular uptake behavior of free Cou-6, Cou-6 LPs, PEI@Cou-6 LPs and PEI-FA@Cou-6 LPs incubated with 4T1 cells by CLSM imaging. (Scale bar: 100 μ m) (E) Cellular uptake behavior of PEI-FA@Cou-6 LPs (FA+) and PEI-FA@Cou-6 LPs (FA-) incubated with 4T1, A2780, bEND.3 cells by CLSM imaging. (F) Cellular uptake and (G) the mean fluorescence intensity analysis of free Cou-6, Cou-6 LPs, PEI@Cou-6 LPs and PEI-FA@Cou-6 LPs incubated with 4T1 cells by flow cytometry. (H) Quantification analysis of PEI-FA@Cou-6 LPs (FA+) and PEI-FA@Cou-6 LPs (FA-) incubated with 4T1 cells by flow cytometry. (Scale bar: 100 μ m) Data are shown as mean \pm SD ($n=3$). The unpaired student t test was used to estimate statistical significance of differences between groups. ** $P < 0.01$, *** $P < 0.001$

In vitro anticancer efficacy of liposomes

The cytotoxicity of Blank LPs and PEI-FA@Blank LPs was measured in 4T1 cells using CCK-8 assays. As shown in Fig. 5A, both Blank LPs and PEI-FA@Blank LPs exhibited minimal cytotoxicity in 4T1 cells, with survival rates exceeding 85% after 24–48 h of treatment. Thus, the Blank LPs are safe and biocompatible for in vivo

applications. As shown in Fig. 5B, drug-loaded LPs had potent cytotoxic effects after light irradiation. Irradiated PEI-FA@IR@TPZ/BMS LPs were more cytotoxic to 4T1 cells than unirradiated LPs. The increased cytotoxicity was due to the elevated production of ROS and increased hypoxia on the cell surface after irradiation,

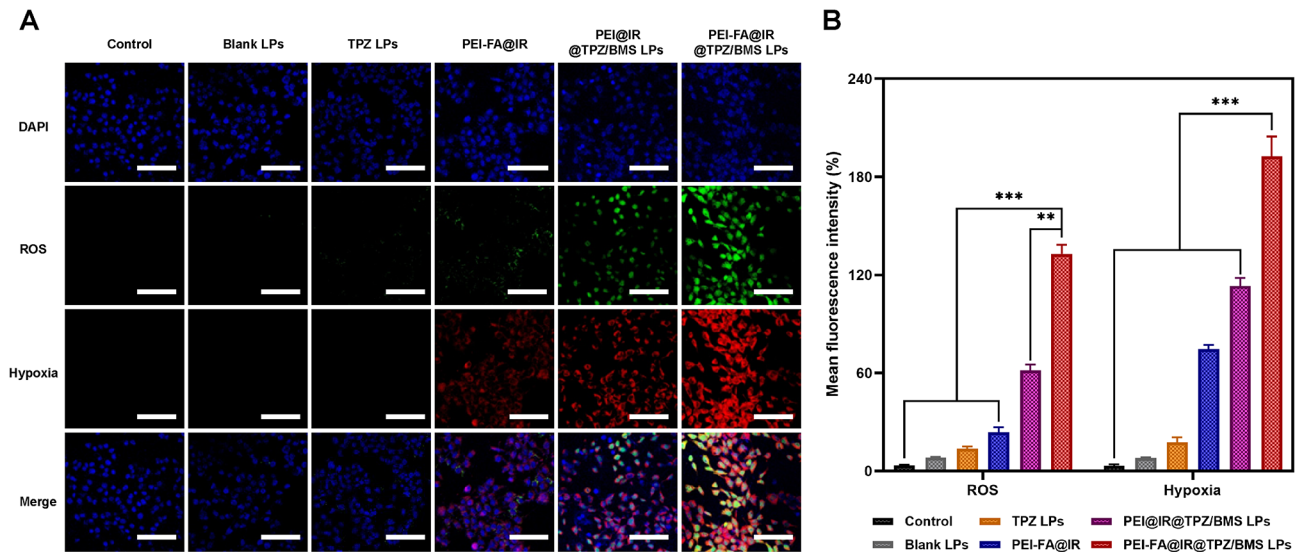


Fig. 4 In vitro detection of ROS/hypoxia. **(A)** In vitro detection of ROS/hypoxia in differently treated 4T1 cells (Scale bar: 100 μ m). **(B)** Quantification of in vitro detection of ROS/hypoxia. Data are shown as mean \pm SD ($n = 3$). The unpaired student t test was used to estimate statistical significance of differences between groups. $**P < 0.01$, $***P < 0.001$

which potentiated the cytotoxicity of TPZ, resulting in decreased tumor cell viability.

Apoptosis was detected using Annexin V-FITC/PI double staining, as depicted in Fig. 5C and D. The apoptosis ratio of irradiated cells was significantly higher than that of unirradiated cells after 48 h of culture. Notably, PEI-FA@IR@TPZ/BMS LPs exhibited a significantly higher cell apoptosis ratio than the other groups. This difference was attributed to the active targeting effect of FA. Moreover, IR820 irradiation induced more hypoxia, intensifying the effect of TPZ on tumor cells. In the unirradiated groups, the apoptosis rates were 13.4% for TPZ LPs, 9.91% for BMS LPs, 17.1% for PEI@IR@TPZ/BMS LPs, and 31.3% for PEI-FA@IR@TPZ/BMS LPs. In the irradiated groups, the apoptosis rates were 24.9% for TPZ LPs, 22.2% for BMS LPs, 47.1% for PEI@IR@TPZ/BMS LPs, and 48.0% for PEI-FA@IR@TPZ/BMS LPs. These results suggest that PEI-FA@IR@TPZ/BMS LPs promote the apoptosis of 4T1 cells, with FA-modified lipid nanoparticles exhibiting stronger apoptotic activity than PEI@IR@TPZ/BMS LPs due to their active targeting effect. Light exposure enhanced the apoptotic effects of TPZ.

The calcein-AM/PI co-staining results support the cell inhibition and apoptosis results. Red fluorescence indicated dead cells, and green fluorescence represented live cells. In the absence of irradiation (Fig. 5E and F), significant red fluorescence was not detected in any treatment groups. However, irradiation increased red fluorescence, indicating more dead cells. The apoptosis rates in illuminated cells were 11.2% for TPZ LPs, 16.9% for BMS LPs, 48.3% for PEI@IR@TPZ/BMS LPs, and 72.5% for PEI-FA@IR@TPZ/BMS LPs. Notably, PEI-FA@IR@TPZ/BMS LPs induced the highest level of cell

death, indicating a robust anti-tumor effect. These results were consistent with the outcomes of the flow cytometry analysis.

In vitro immune response

PDT induces ICD, which is characterized by the release of damage-associated molecular patterns (DAMPs) from dead tumor cells. DAMPs activate tumor-specific immune responses that contribute to the long-term effectiveness of anticancer drugs through a combination of direct killing of cancer cells and antitumor immunity [25]. Therefore, the effectiveness of cell-mediated immune responses can be assessed by measuring ATP and CRT levels. Tumor cell necrosis or apoptosis following PDT results in the exposure of ATP and CRT, initiating the immune process [26]. CRT expression in 4T1 cells in response to PDT was visualized by fluorescence, as shown in Fig. 6A. In the absence of laser irradiation, negligible fluorescence signals were observed. However, treatment with PEI-FA@IR@TPZ/BMS LPs induced the highest CRT expression, characterized by a bright red color. As shown in Fig. 6B, ATP release from PEI@IR@TPZ/BMS LPs (556.18 nM) in response to laser irradiation was significantly higher than ATP release in the respective unirradiated group. Similarly, HMGB1 release from cells treated with PEI@IR@TPZ/BMS LPs was significantly higher after light exposure (768.75 pg/mL) than HMGB1 release from cells treated with PEI@IR@TPZ/BMS LPs without light exposure (368.75 pg/mL) (Fig. 6C). In summary, the CRT, ATP, and HMGB1 results confirmed that PEI@IR@TPZ/BMS LPs induced robust ICD and a systemic immune response.

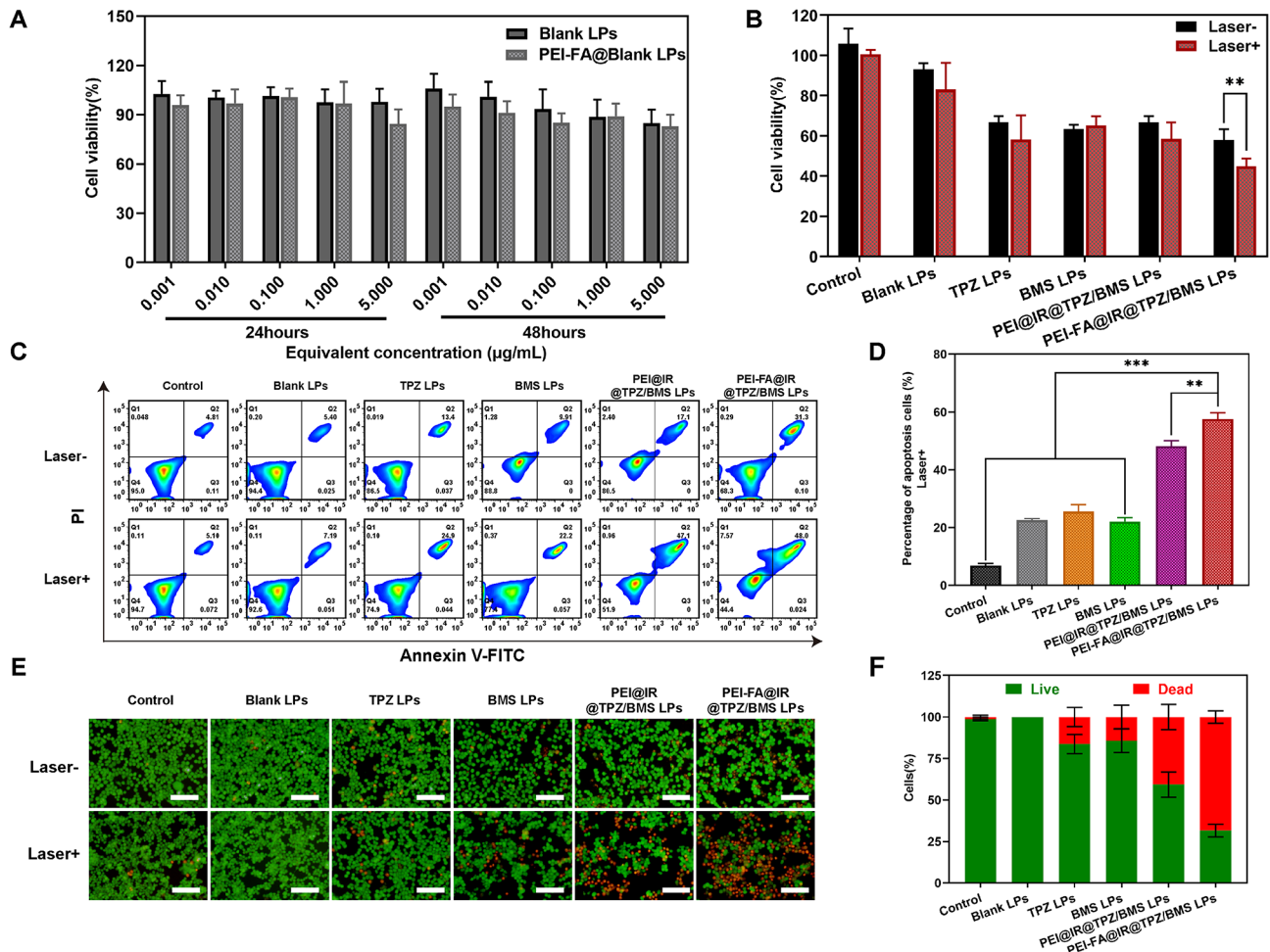


Fig. 5 In vitro anti-cancer study. **(A)** In vitro cytotoxicity of Blank LPs and PEI-FA@Blank LPs on 4T1 cells. **(B)** Inhibitory capacity of different groups treated against 4T1 cells proliferation. Cell apoptosis assay on 4T1 cells in vitro. **(C, D)** The flow cytometry results of 4T1 cells apoptosis and the percentage of early and late apoptosis after the 48 h treatment and near-infrared laser irradiation with different treatments. **(E, F)** Live/dead examination of 4T1 cells subjected to different treatments was conducted using Calcein-AM/PI double staining and observing by inverted fluorescence microscope (Scale bar: 100 µm). Data are shown as mean ± SD ($n=3$). The unpaired student t test was used to estimate statistical significance of differences between groups. ** $P < 0.01$, *** $P < 0.001$

Biodistribution of liposomes in vivo

FA-mediated antitumor agents specifically target folate receptor-positive tumor cells [27]. To evaluate the distribution and accumulation efficacy of PEI-FA@IR@TPZ/BMS LPs in various organs, we constructed the 4T1 tumor-bearing mouse model, prepared PEI@IR@TPZ/BMS LPs and PEI-FA@IR@TPZ/BMS LPs respectively, and compared the in vivo targeting efficacy through the in vivo imaging system. It can be seen from the in vivo distribution results that PEI-FA@IR@TPZ/BMS LPs have better tumor targeting than PEI@IR@TPZ/BMS LPs (Fig. 7A and B). It can be seen from the internal organ distribution results (Fig. 7C and D) that the accumulation of LPs modified by PEI in the heart, liver, spleen, lung and kidney is more than that in PEI-FA@IR@TPZ/BMS LPs. This may be due to the strong positive charge on the surface of PEI, which can accumulate to various organs and

parts without selectivity, causing systemic distribution. The non-selective distribution of the whole body can be reduced after FA modification, and thus improved active targeting in tumor sites.

In vivo ROS generation efficiency

In order to determine the effect of ROS generated by IR820, we observed the levels of DCFH-DA in vivo. As can be seen in Figure S5, strong green fluorescence of DCF was detected throughout the tumor sections of the PEI-FA@IR@TPZ/BMS LPs under irradiation groups, indicating ROS generation in vivo. However, negligible levels of DCF green fluorescence was observed in the control group and the non-irradiated PEI-FA@IR@TPZ/BMS LPs, indicating that the IR820 photosensitizer in the PEI-FA@IR@TPZ/BMS LPs was successfully excited under infrared irradiation and produced ROS in vivo.

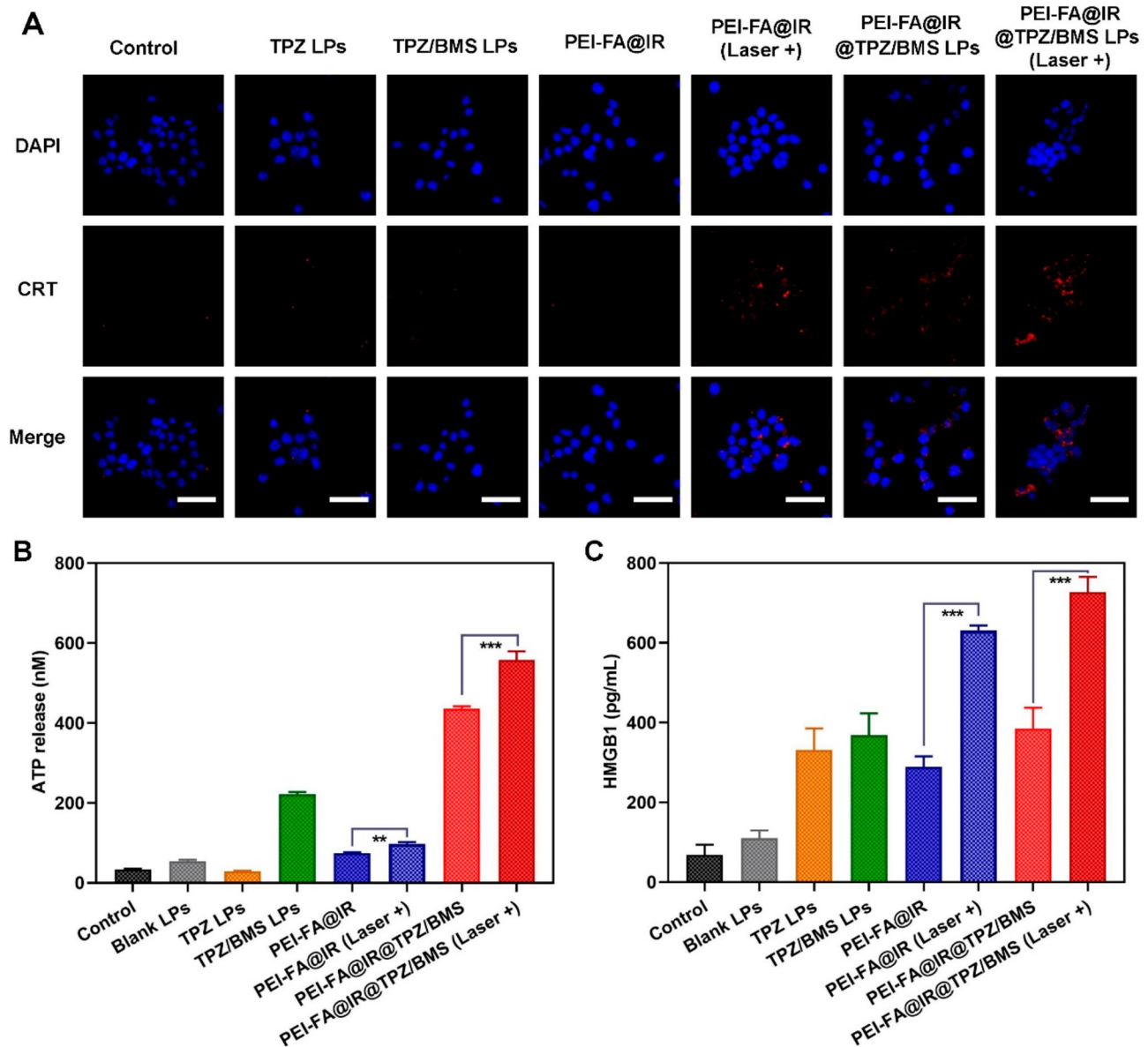


Fig. 6 Analysis of in vitro ICD biomarkers on 4T1 cells. **(A)** In vitro detection of CRT in differently treated 4T1 cells (Scale bar: 50 μ m). **(B)** The release of ATP from 4T1 cells subjected to different treatments. **(C)** The release of HMGB1 from 4T1 cells subjected to different treatments. Data are shown as mean \pm SD ($n=3$). The unpaired student t test was used to estimate statistical significance of differences between groups. $**P < 0.01$, $***P < 0.001$

In vivo antitumor and safety evaluation

We assessed the anticancer efficacy of PEI-FA@IR@TPZ/BMS LPs in a highly metastatic mouse breast cancer model. Figures S6, 8A, and B demonstrates that both the saline and Blank LPs groups were ineffective in inhibiting tumor growth. TPZ LPs, BMS LPs, and PEI-FA@IR groups showed only minimal inhibitory effects on tumor growth, indicated that these three drugs cannot achieve outstanding anti-tumor efficacy when administered separately. However, when these three drugs were delivered to the tumor using the same co-delivery vector, significant anti-tumor efficacy was observed. PEI@IR@TPZ/BMS LPs and PEI-FA@IR@TPZ/BMS LPs groups exhibited

significantly stronger antitumor effects than the other treatment groups. Between PEI@IR@TPZ/BMS LPs and PEI-FA@IR@TPZ/BMS LPs groups, the anti-tumor efficacy of PEI-FA@IR@TPZ/BMS LPs group was significantly improved than that of PEI@IR@TPZ/BMS LPs group due to the active targeting effect of the FA. The tumor growth inhibition rate in each treatment was 2.91% (Blank LPs), 24.27% (TPZ LPs), 40.29% (BMS LPs), 26.21% (PEI-FA@IR), 53.88% (PEI@IR@TPZ/BMS LPs), and 68.81% (PEI-FA@IR@TPZ/BMS LPs) respectively. Furthermore, TUNEL staining of tumor tissues corroborated the anticancer efficacy of the LPs. As illustrated in

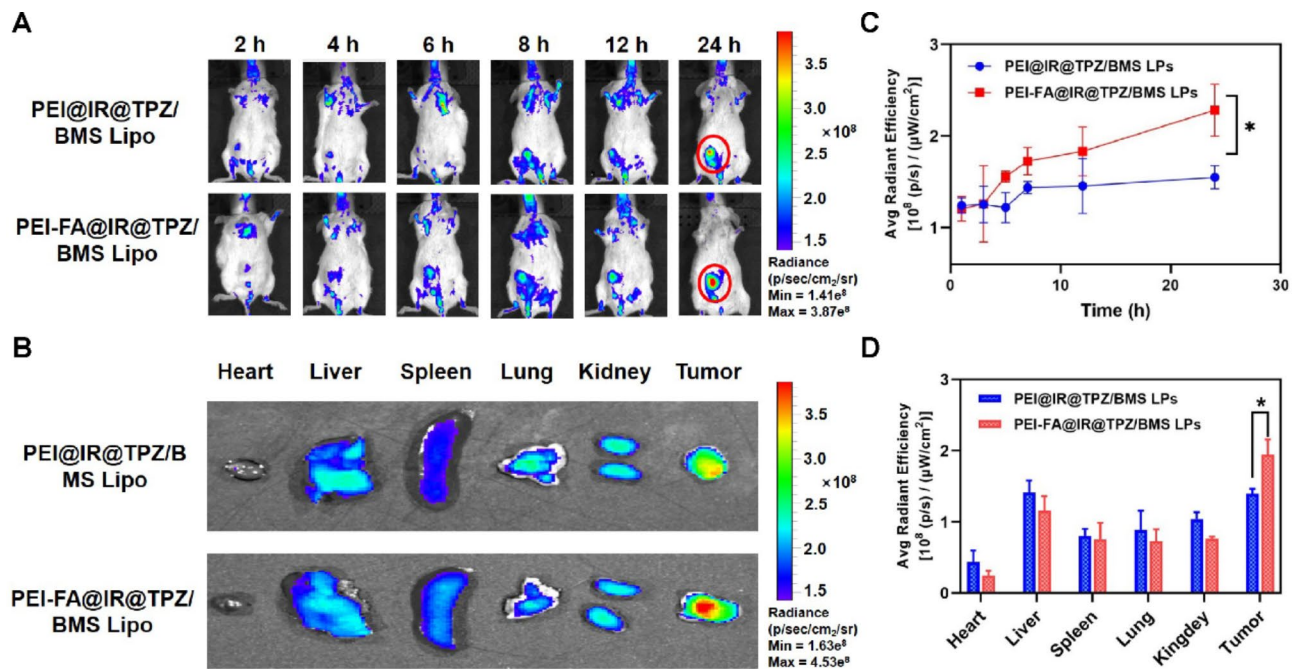


Fig. 7 Biodistribution of PEI-FA@IR@TPZ/BMS LPs in vivo. **(A)** In vivo fluorescence images of 4T1-bearing BALB/c mice treated with PEI@IR@TPZ/BMS LPs and PEI-FA@IR@TPZ/BMS LPs. Images were taken at 2, 4, 6, 8, 12, and 24 h after injection. **(B)** Quantitative analysis of Fig. **(A)** in tumors. **(C)** The fluorescence images of the excised tumors and major organs at 24 h after injection. **(D)** Quantitative analysis of the kinetic fluorescence intensity in excised tumors and organs. Data are shown as mean \pm SD ($n=3$). The unpaired student t test was used to estimate statistical significance of differences between groups, $*P < 0.05$

Fig. 8C, only a few apoptotic cells were detected in mice treated with saline. Small numbers of apoptotic cells were detected in mice treated with single drugs or Blank LPs. In contrast, a high number of apoptotic tumor cells were detected in mice treated with PEI-FA@IR@TPZ/BMS LPs. The proportion of apoptotic cells in each group correlated with the tumor volume curve, confirming the superior tumor growth inhibition and apoptotic properties of PEI-FA@IR@TPZ/BMS LPs over the other treatment groups.

This phenomenon may be closely linked to TPZ-induced hypoxia-activated chemotherapy. To validate this hypothesis, HIF- α levels were assessed in tumor tissues. As shown in Fig. 8C, HIF- α staining indicated more hypoxia in tumors from mice treated with PEI@IR@TPZ/BMS LPs and PEI-FA@IR@TPZ/BMS LPs compared with hypoxia in the tumor tissues of mice treated with TPZ LPs or BMS LPs. These results suggest that the effective accumulation of these agents at the tumor site, along with IR820, led to more oxygen depletion. Taken together, these results suggest that treatment with PEI-FA@IR@TPZ/BMS LPs combined with 808 nm laser irradiation exacerbates tumor hypoxia. Hypoxia activates the hypoxia-sensitive drug TPZ, resulting in the dual antitumor effects of phototherapy and hypoxia-activated chemotherapy. In addition, we investigated the expression levels of PD-L1 in tumor tissues of different formulation

groups. The expression of PD-L1 in the tumor tissue of mice treated with PEI-FA@IR@TPZ/BMS LPs was significantly reduced, indicating that BMS successfully blocked the expression of PD-L1 on the surface of tumor cells in vivo, reduced its binding with immune cells, and further promoted anti-tumor immunotherapy under the combined effect of chemotherapy and phototherapy, ultimately achieving efficient anti-tumor efficacy under multiple mechanisms.

To investigate the effect of PEI-FA@IR@TPZ/BMS LPs on tumor metastasis, the lungs of mice were fixed in Bouin's solution after the final treatment. As shown in Fig. 8D, several white lung nodules, indicating tumor metastasis, were observed in the control group. However, minimal significant pulmonary metastatic nodules were observed in mice treated with PEI-FA@IR@TPZ/BMS LPs, indicating the effectiveness of these LPs in preventing tumor metastasis. To assess the systemic toxicity of the various agents, we monitored mouse body weight and serum biochemical indices and examined the major organs after treatment. Mouse body weights were stable, with no significant weight loss in any group (Fig. 9A). As shown in Fig. 9B, serum biochemical indices were not significantly different among the treatment groups, indicating that PEI-FA@IR@TPZ/BMS LPs did not compromise liver or kidney function. As shown in Fig. 9C, H&E staining revealed no signs of tissue damage or tumor

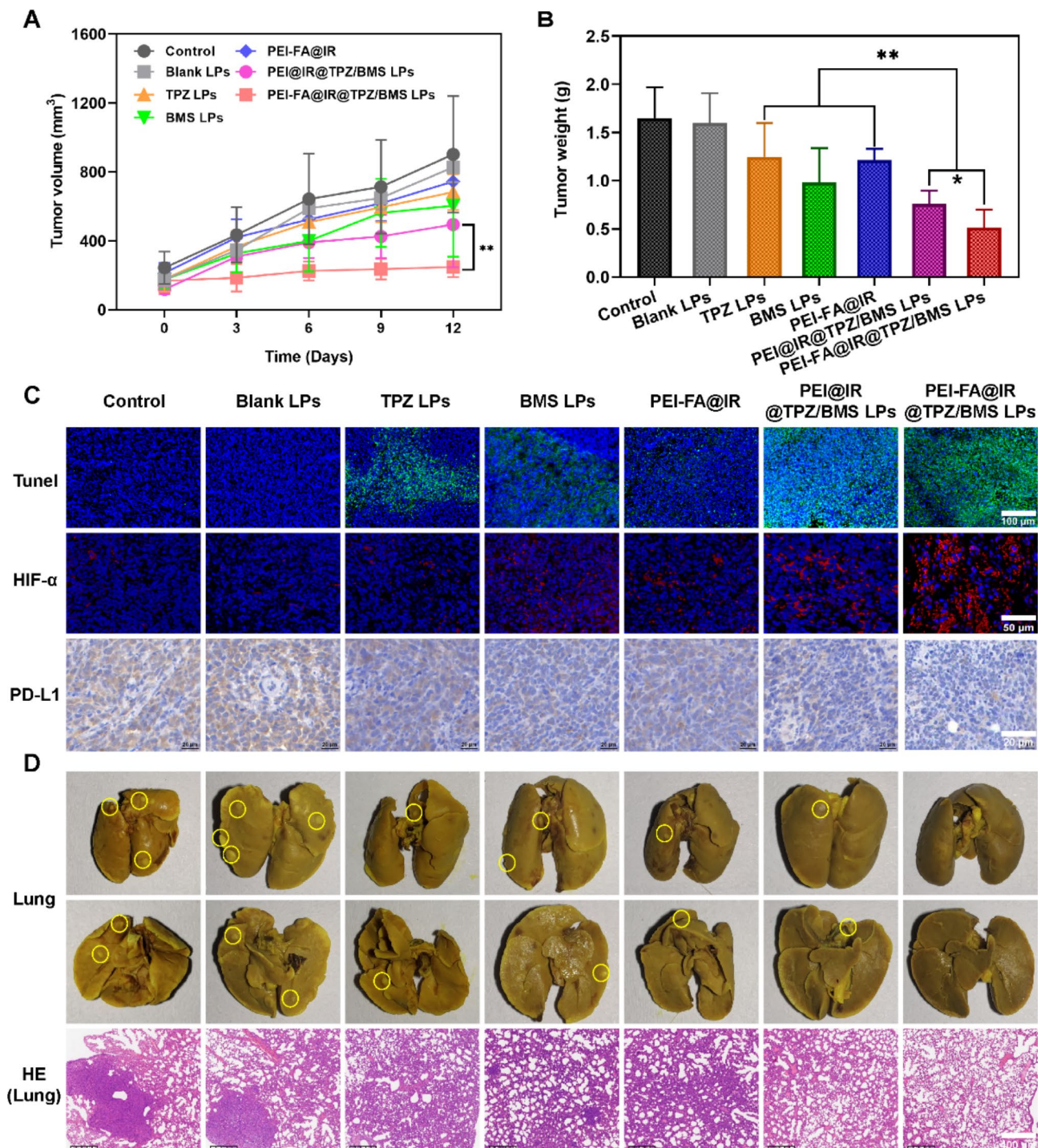


Fig. 8 Antitumor Evaluation of PEI-FA@IR@TPZ/BMS LPs in vivo. The 4T1-bearing BALB/c mice were treated with Saline, Blank LPs, TPZ LPs, BMS LPs, PEI-FA@IR, PEI@IR@TPZ/BMS LPs, and PEI-FA@IR@TPZ/BMS LPs. **(A)** Tumor volume of mice. **(B)** Weight of isolated tumors. **(C)** TUNEL assay (Scale bar: 100 μ m), HIF- α assay (Scale bar: 50 μ m) and PD-L1 assay (Scale bar: 20 μ m) of tumor tissues isolated from mice. **(D)** Bouin's staining and H&E staining of lung isolated from mice (Scale bar: 400 μ m). Data are shown as mean \pm SD ($n=5$). The unpaired student t test was used to estimate statistical significance of differences between groups. * $P < 0.05$, ** $P < 0.01$

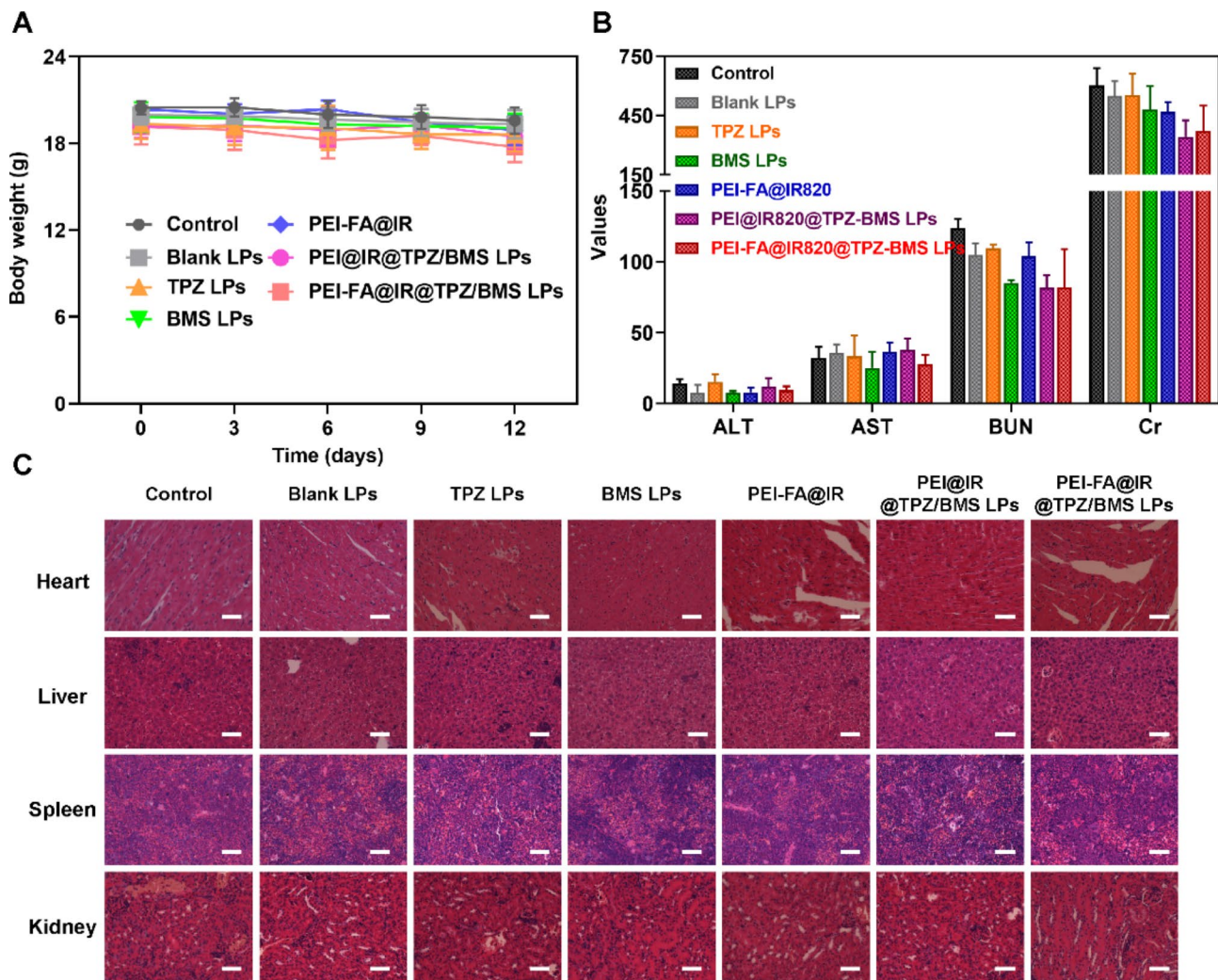


Fig. 9 In vivo safety and anti-metastasis evaluation of PEI-FA@IR@TPZ/BMS LPs in vivo. The 4T1-bearing BALB/c mice were treated with Saline, Blank LPs, TPZ LPs, BMS LPs, PEI-FA@IR, PEI@IR@TPZ/BMS LPs, and PEI-FA@IR@TPZ/BMS LPs. **(A)** Body weight of mice. **(B)** ALT, AST, BUN and Cr from the blood samples isolated from mice. **(C)** H&E staining of organs isolated from mice (Scale bar: 200 μ m). Data are shown as mean \pm SD ($n=5$)

metastasis in the hearts, livers, spleens, or kidneys of mice in any group. These findings validate the biocompatibility and safety of PEI-FA@IR@TPZ/BMS LPs.

In vivo antitumor immune response

The effects of combined chemotherapy and PDT in remodeling the tumor microenvironment (TME) in vivo were examined using flow cytometry to detect T-cell expression in mouse tumor cells. Ths (CD3+CD4+CD8-) and CTLs (CD3+CD4-CD8+) play pivotal roles in immune regulation. Effective cancer immunotherapy initiates and supports T cells to generate a lasting antitumor response [28]. CD4+T cells also initiate a gene expression program in CD8+T cells to enhance CTL function, enabling CTLs to overcome barriers to antitumor immunity [29].

As shown in Fig. 10A and E, the percentage of intratumoral CD3+CD4+T cells significantly increased, reaching an astonishing 18% after treatment with PEI-FA@IR@TPZ/BMS LPs and levels were 2.09-fold, 1.59-fold, 1.80-fold, and 1.39-fold higher than in mice treated with TPZ LPs, BMS LPs, PEI-FA@IR, and PEI@IR@TPZ/BMS LPs, respectively. Furthermore, PEI-FA@IR@TPZ/BMS LPs group exhibited higher levels of CD3+CD8+T cells than the other groups. As shown in Fig. 10B and E, following treatment with PEI@IR@TPZ/BMS LPs, the percentage of CD3+CD8+T cells in tumor tissues was measured at 25.9%. This level exhibited a 2.71-fold increase compared to mice treated with TPZ LPs, a 2.21-fold increase compared to those treated with BMS LPs, a 1.88-fold increase compared to PEI-FA@IR, and nearly a 2-fold increase compared to PEI@IR@TPZ/BMS LPs. These results suggest that the combined use of a PD-1/PD-L1 inhibitor

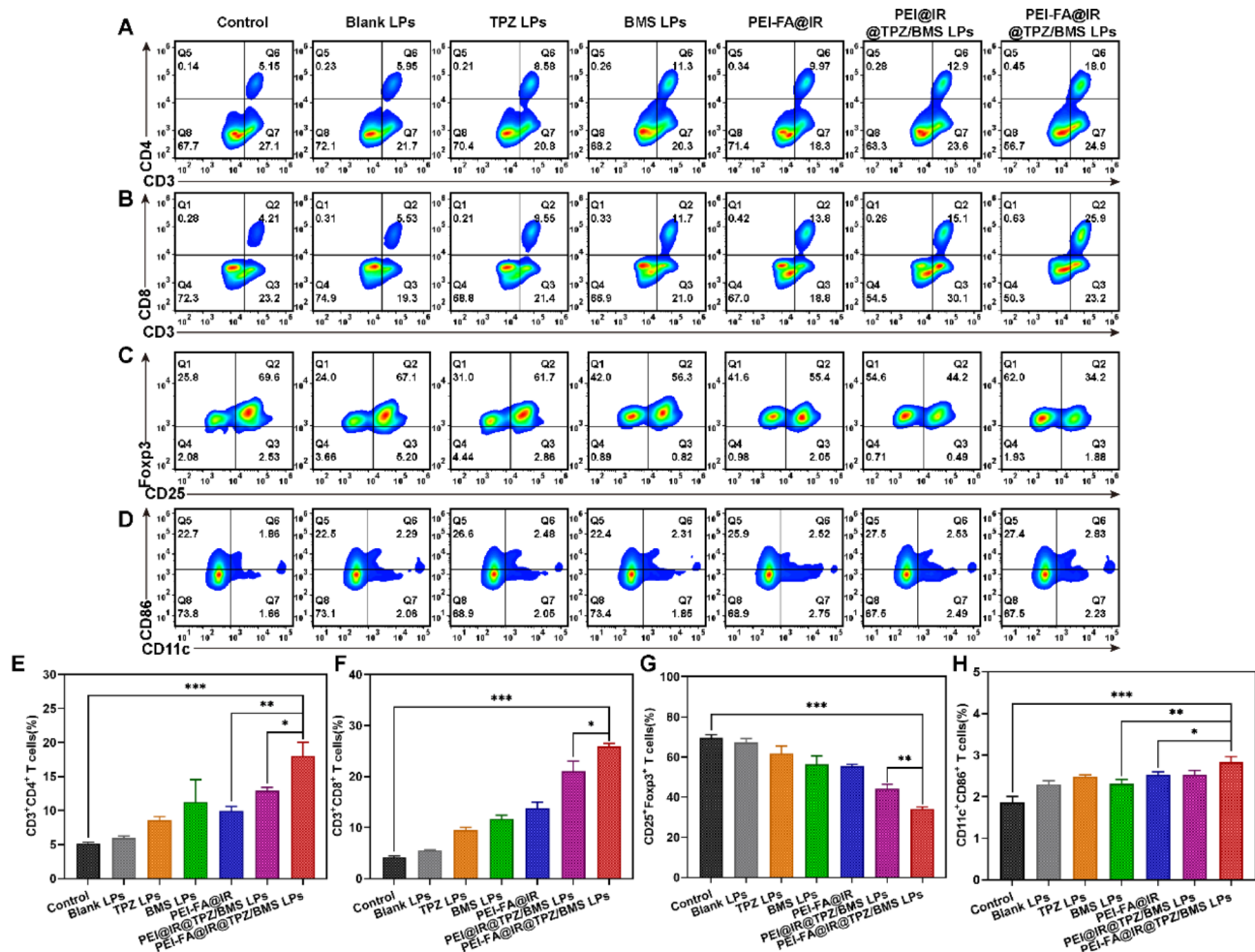


Fig. 10 Immune Response Analysis of PEI-FA@IR@TPZ/BMS LPs in a 4T1-bearing BALB/c mice tumor model. **(A)** Flow cytometric analysis and **(E)** Quantification analysis of Ths (CD3+CD4+CD8-) in tumor. **(B)** Flow cytometric analysis and **(F)** Quantification analysis of CTLs (CD3+CD4-CD8+) in tumor. **(C)** Flow cytometric analysis and **(G)** Quantification analysis of Tregs (CD4+CD25+Foxp3+) in tumor. **(D)** Flow cytometric analysis and **(H)** Quantification analysis of DCs (CD45+CD11c+CD86+) cells in spleen. Data are shown as mean \pm SD ($n=5$). The unpaired student t test was used to estimate statistical significance of differences between groups. * $P < 0.05$, ** $P < 0.01$, *** $P < 0.001$

(BMS), a chemotherapeutic agent (TPZ), and a photosensitizer (IR820) disrupted the immune-suppressive effects of PD-1/PD-L1, reversed T-cell exhaustion in the TME, activated CD4+CD8+ T cells, and enhanced the immune response within the tumor. IHC results confirmed the flow cytometry results (Fig. 11A), displaying maximal positive expression in PEI-FA@IR@TPZ/BMS LPs.

Tregs (CD4+CD25+FOXP3+) suppress T cells, and tumor-specific CD4+T cells in the TME can be reprogrammed into Tregs, counteracting CTL activity and delaying immune responses [30]. As shown in Fig. 10C and G, both PEI@IR@TPZ/BMS LPs and PEI-FA@IR@TPZ/BMS LPs significantly decreased Foxp3+ levels. The proportion of Tregs in PEI-FA@IR@TPZ/BMS LPs could be inhibited to 34.2%. This suggests that lipid nanoparticles encapsulating BMS can suppress the number of Tregs to enhance immune responses.

In addition to local immunity at the tumor site, a robust systemic immune response is crucial for exerting antitumor immunity. Therefore, the expression levels of DCs (CD11c+CD45+CD86+) in the spleen were assessed after the last treatment. DCs, as specialized antigen-presenting cells, play a crucial role in activating and regulating the immune response [31]. As a key component of antitumor responses, mature DCs can present tumor antigens to T-cell receptors, promoting T-cell activation and infiltration into the tumor site [30]. As shown in Fig. 10D and H, PEI-FA@IR@TPZ/BMS LPs promoted DC maturation 1.14-fold, 1.22-fold, 1.12-fold, and 1.12-fold more than TPZ LPs, BMS LPs, PEI-FA@IR, and PEI@IR@TPZ/BMS LPs, respectively. In summary, the successful performance of PEI-FA@IR@TPZ/BMS LPs in inducing PDT-mediated ICD under laser irradiation highlights the benefits of the synergistic approach involving tumor metabolism reprogramming and PDT therapy.

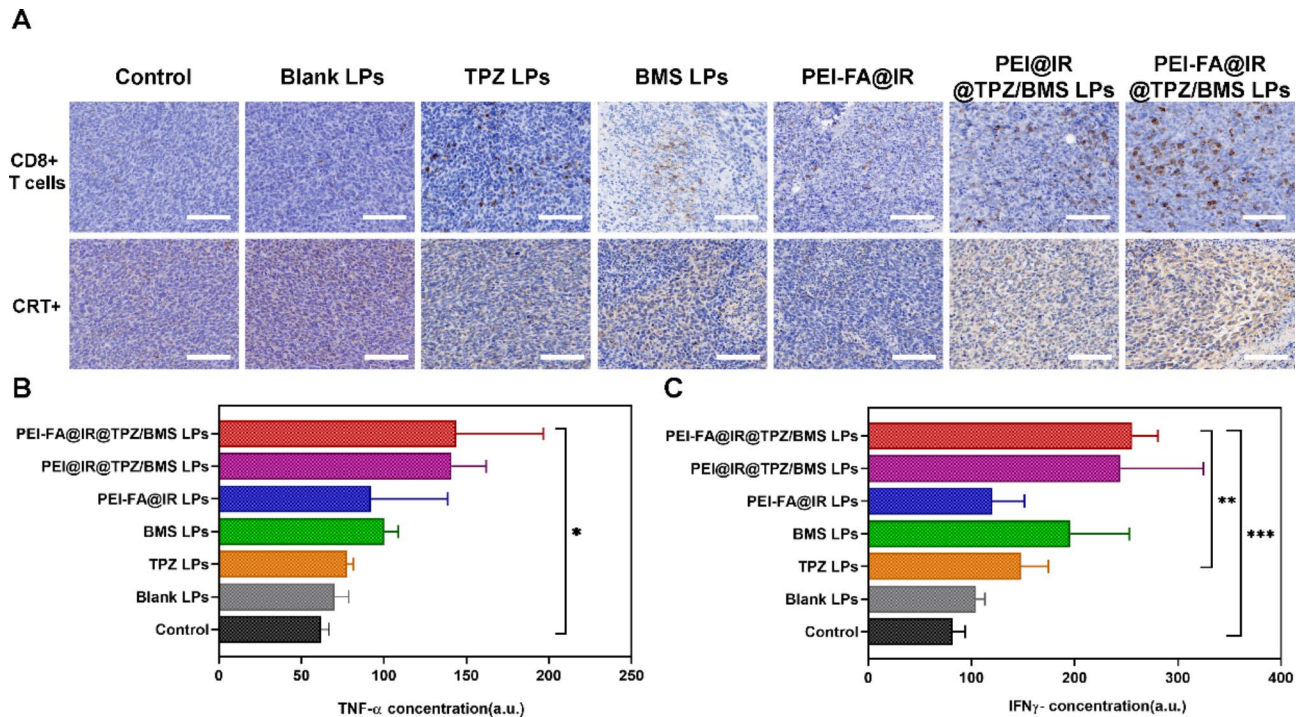


Fig. 11 Immune Response Analysis of PEI-FA@IR@TPZ/BMS LPs in a 4T1-bearing BALB/c mice tumor model. **(A)** CD8+T cells and CRT staining for tumor tissue slices of different groups (Scale bar: 100 μ m). **(B)** TNF- α and **(C)** IFN- γ levels in tumor tissues in the mice using ELISA kits. Data are shown as mean \pm SD ($n=5$). The unpaired student t test was used to estimate statistical significance of differences between groups. * $P < 0.05$, ** $P < 0.01$, *** $P < 0.001$

Finally, the expression levels of TNF- α and IFN- γ were measured in the serum of mice from each treatment group [30]. TNF- α is a cytokine with tumor necrotic activity [32], and IFN- γ is a key regulator of cell-mediated immunity [33]. As illustrated in Fig. 11B and C, serum TNF- α and IFN- γ levels increased in all treatment groups compared than the control group; TNF- α and IFN- γ levels increased 2.32 and 3.12 times higher, respectively, in mice treated with PEI-FA@IR@TPZ/BMS LPs than in those treated with saline. IFN- γ levels did not increase significantly in mice treated with TPZ LPs or PEI-FA@IR compared with the other groups, suggesting that PD-L1 upregulation suppressed CTLs. However, BMS LPs, PEI@IR@TPZ/BMS LPs, and PEI-FA@IR@TPZ/BMS LPs groups successfully restored antitumor immunity in vivo by inhibiting the PD-1/PD-L1 pathway effects with BMS, upregulating CTL infiltration, and increasing serum TNF- α and IFN- γ levels. These findings indicate that combining PEI-FA@IR@TPZ/BMS LPs, chemotherapy, and PDT greatly enhances the antitumor immune responses.

Conclusions

In this current research, we have engineered multi-functional lipid nanoparticles tailored for breast cancer therapy. This innovative formulation demonstrates exceptional capabilities in drug delivery efficiency, responsiveness to chemotherapy within hypoxic environments, and

elicitation of potent ICD responses. Combining IR820 and TPZ enabled the efficient combination of PDT treatment and hypoxia-activated chemotherapy. More importantly, the liposomal nanodelivery system loaded with BMS enhanced tumor CTLs penetration, yielding effective tumor chemo-immunotherapy in a breast tumor mouse model. In addition, the nanodelivery platform exhibited long-circulating pharmacokinetic properties and low systemic toxic effects. Therefore, LPs loaded with multiple drugs integrated chemotherapy, PDT, and immunotherapy onto a nanoplatform. This effective anti-cancer approach has great potential for improving the outcomes of breast cancer patients.

Supplementary Information

The online version contains supplementary material available at <https://doi.org/10.1186/s12951-024-02838-1>.

Supplementary Material 1

Acknowledgements

We acknowledge the support from the National Natural Science Fund for Distinguished Young Scholars (82104106), the National Natural Science Foundation of China (82073778).

Author contributions

B.Z.: Conceptualization, Methodology, Writing-original draft preparation. L.P.: Investigation, Software. Y.L.: Software, Validation. S.W.: Software, Resources. N.W.: Software, Validation. C.L.: Investigation. H.W.: Investigation. H.W.: Investigation. L.C.: Supervision, Resources. W.H.: Supervision, Resources. Z.G.:

Writing – review & editing, Funding acquisition. X.Y.: Validation, Supervision, Resources. M.J.: Writing – review & editing, Validation, Funding acquisition.

Data availability

No datasets were generated or analysed during the current study.

Declarations

Competing interests

The authors declare no competing interests.

Author details

¹State Key Laboratory of Bioactive Substance and Function of Natural Medicines, Institute of Materia Medica, Chinese Academy of Medical Sciences and Peking Union Medical College, Beijing 100050, China

²Beijing Key Laboratory of Drug Delivery Technology and Novel Formulations, Institute of Materia Medica, Chinese Academy of Medical Sciences and Peking Union Medical College, Beijing 100050, China

³Department of Gynecology and Obstetrics, Yanbian University Hospital, Yanji, Jilin 133000, People's Republic of China

⁴Department of Pharmacy, Yanbian University, Yanji Jilin 133000, P.R. China

Received: 26 March 2024 / Accepted: 5 September 2024

Published online: 12 September 2024

References

1. Trapani D, et al. Global challenges and policy solutions in breast cancer control. *Cancer Treat Rev.* 2022;104:102339.
2. Jin M, et al. Smart polymeric nanoparticles with pH-responsive and PEG-detachable properties for co-delivering paclitaxel and survivin siRNA to enhance antitumor outcomes. *IJN Volume.* 2018;13:2405–26.
3. Traves KP, Cokenakes SEH. Breast Cancer Treatment. *Am Fam Physician.* 2021;104:171–8.
4. Riley RS, June CH, Langer R, Mitchell M. J. Delivery technologies for cancer immunotherapy. *Nat Rev Drug Discov.* 2019;18:175–96.
5. Combination. strategies with PD-1/PD-L1 blockade: current advances and future directions - PubMed. <https://pubmed.ncbi.nlm.nih.gov/35062949/>
6. Fang W, et al. Progranulin induces immune escape in breast cancer via up-regulating PD-L1 expression on tumor-associated macrophages (TAMs) and promoting CD8+T cell exclusion. *J Exp Clin Cancer Res.* 2021;40:4.
7. Immune induction strategies. In metastatic triple-negative breast cancer to enhance the sensitivity to PD-1 blockade: the TONIC trial - PubMed. <https://pubmed.ncbi.nlm.nih.gov/31086347/>
8. Santoni M, et al. Triple negative breast cancer: key role of Tumor-Associated macrophages in regulating the activity of anti-PD-1/PD-L1 agents. *Biochim Biophys Acta Rev Cancer.* 2018;1869:78–84.
9. Bastaki S, et al. PD-L1/PD-1 axis as a potent therapeutic target in breast cancer. *Life Sci.* 2020;247:117437.
10. Structural Biology of the Immune Checkpoint Receptor PD-1. and Its Ligands PD-L1/PD-L2 - PubMed. <https://pubmed.ncbi.nlm.nih.gov/28768162/>
11. BMS-202. A PD-1/PD-L1 inhibitor, decelerates the pro-fibrotic effects of fibroblasts derived from scar tissues via ERK and TGFβ1/Smad signaling pathways - PubMed. <https://pubmed.ncbi.nlm.nih.gov/36169254/>
12. Lin L, Song X, Dong X, Li B. Nano-photosensitizers for enhanced photodynamic therapy. *Photodiagnosis Photodyn Ther.* 2021;36:102597.
13. Dash BS, Das S, Chen J-P. Photosensitizer-functionalized nanocomposites for light-activated Cancer Theranostics. *Int J Mol Sci.* 2021;22:6658.
14. Wan Y, Fu L-H, Li C, Lin J, Huang P. Conquering the Hypoxia limitation for photodynamic therapy. *Adv Mater.* 2021;33:e2103978.
15. Reddy SB, Williamson SK. Tirapazamine: a novel agent targeting hypoxic tumor cells. *Expert Opin Investig Drugs.* 2009;18:77–87.
16. Li Y, Zhao L, Li X-F. Targeting Hypoxia: Hypoxia-activated Prodrugs in Cancer Therapy. *Front Oncol.* 2021;11:700407.
17. Almeida B, Nag OK, Rogers KE, Delehanty JB. Recent progress in Bioconjugation strategies for liposome-mediated drug delivery. *Molecules.* 2020;25:5672.
18. Wang S, et al. Hollow mesoporous silica nanoparticles-loaded ion-crosslinked bilayer films with excellent mechanical properties and high bioavailability for buccal delivery. *Int J Pharm.* 2022;624:122056.
19. Wang S, Meng S, Zhou X, Gao Z, Piao MG. pH-Responsive and mucoadhesive nanoparticles for enhanced oral insulin delivery: the Effect of Hyaluronic Acid with different molecular weights. *Pharmaceutics.* 2023;15:820.
20. Itoo AM, Paul M, Padaga SG, Ghosh B, Biswas S. Nanotherapeutic intervention in photodynamic therapy for Cancer. *ACS Omega.* 2022;7:45882–909.
21. Jin M, et al. Smart Polymeric nanoparticles with pH-Responsive and PEG-Detachable properties (II): Co-delivery of Paclitaxel and VEGF siRNA for synergistic breast Cancer Therapy in mice. *IJN Volume.* 2021;16:5479–94.
22. Hou Y. Targeted therapeutic effects of oral inulin-modified double-layered nanoparticles containing chemotherapeutics on orthotopic colon cancer. (2022).
23. Solak K, Mavi A, Yilmaz B. Disulfiram-loaded functionalized magnetic nanoparticles combined with copper and sodium nitroprusside in breast cancer cells. *Mater Sci Engineering: C.* 2021;119:111452.
24. Wang S, et al. Preparation, in vitro and in vivo evaluation of chitosan-sodium alginate-ethyl cellulose polyelectrolyte film as a novel buccal mucosal delivery vehicle. *Eur J Pharm Sci.* 2022;168:106085.
25. Ahmed A, Tait SWG. Targeting immunogenic cell death in cancer. *Mol Oncol.* 2020;14:2994–3006.
26. Krysko DV, et al. Immunogenic cell death and DAMPs in cancer therapy. *Nat Rev Cancer.* 2012;12:860–75.
27. Wan L, et al. Folate-Polyethyleneimine functionalized mesoporous carbon nanoparticles for enhancing oral bioavailability of paclitaxel. *Int J Pharm.* 2015;484:207–17.
28. Borst J, Ahrends T, Bąbala N, Melief CJM, Kastenmüller W. CD4+T cell help in cancer immunology and immunotherapy. *Nat Rev Immunol.* 2018;18:635–47.
29. Ahrends T, et al. CD4+T cell help confers a cytotoxic T cell Effector Program including coinhibitory receptor downregulation and increased tissue invasiveness. *Immunity.* 2017;47:848–e8615.
30. Veglia F, Gabrilovich DI. Dendritic cells in cancer: the role revisited. *Curr Opin Immunol.* 2017;45:43–51.
31. Iberg CA, Hawiger D. Natural and Induced Tolerogenic dendritic cells. *J Immunol.* 2020;204:733–44.
32. Yamazaki M. [TNF-alpha]. *Gan Kagaku Ryoho.* 1994;21:2679–87.
33. Otani N, et al. Changes in cell-mediated immunity (IFN-γ and Granzyme B) following influenza vaccination. *Viruses.* 2021;13:1137.

Publisher's note

Springer Nature remains neutral with regard to jurisdictional claims in published maps and institutional affiliations.